European Journal of Medicinal Chemistry 242 (2022) 114652

Contents lists available at ScienceDirect

European Journal of Medicinal Chemistry

journal homepage: www.elsevier.com/locate/ejmech

Research paper

Development of 3α,7α-dihydroxy-6α-ethyl-24-*nor*-5β-cholan-23-sulfate sodium salt (INT-767): Process optimization, synthesis and characterization of metabolites

Bruno Cerra [a,1], Francesco Venturoni [a,2,1], Maria Souma [a], Giada Ceccarelli [a], Anna Maria Lozza [a], Daniela Passeri [b], Francesca De Franco [b], Ian R. Baxendale [c], Roberto Pellicciari [b], Antonio Macchiarulo [a], Antimo Gioiello [a,*]

[a] Laboratory of Medicinal and Advanced Synthetic Chemistry, Department of Pharmaceutical Sciences, University of Perugia, Via del Liceo 1, 06122, Perugia, Italy
[b] TES Pharma, Via Palmiro Togliatti 20, 06073, Taverne di Corciano, Perugia, Italy
[c] Department of Chemistry, Durham University, South Road, Durham, United Kingdom

ARTICLE INFO

Keywords:
Bile acid
Flow chemistry
FXR
Metabolites
Ozonolysis
Process chemistry
Scale-up
Sulfates

ABSTRACT

Herein we report our synthetic efforts in supporting the development of the bile alcohol sulfate INT-767, a FXR/TGR5 dual agonist with remarkable therapeutic potential for liver disorders. We describe the process development to a final route for large scale preparation and analogues synthesis. Key sequences include Grignard addition, a one-pot two-step shortening-reduction of the carboxylic side chain, and the final sulfation reaction. The necessity for additional steps such as the protection/deprotection of hydroxyl groups at the steroidal body was also evaluated for step-economy and formation of side-products. Critical bottlenecks such as the side chain degradation have been tackled using flow technology before scaling-up individual steps. The final synthetic route may be successfully employed to produce the amount of INT-767 required to support late-stage clinical development of the compound. Furthermore, potential metabolites have been synthesized, characterized and evaluated for their ability to modulate FXR and TGR5 receptors providing key reference standards for future drug investigations, as well as offering further insights into the structure-activity relationships of this class of compounds.

1. Introduction

The compound 3α,7α-dihydroxy-6α-ethyl-24-*nor*-5β-cholan-23-sulfate sodium salt (INT-767, **1**) is a semisynthetic bile acid derivative endowed with FXR agonistic activity and three-fold higher potency than obeticholic acid (OCA, **2**) (Ocaliva™) (Fig. 1a) [1], namely the only FXR agonist so far approved by the FDA for the treatment of primary biliary cholangitis (PBC) [2]. At odds with OCA (**2**), INT-767 (**1**) potently also activates TGR5, a membrane bile acid receptor with a crucial role in modulating metabolic and inflammatory processes, as well as anorexigenic actions of bile acids [3–5]. The pan-agonistic profile of INT-767 (**1**) at the most relevant bile acid receptors and its good physicochemical and preliminary PK profile [6], have prompted several studies to investigate the therapeutic relevance of a selective bile targeting both FXR and TGR5 in gut, liver and renal diseases. Accordingly, promising results have been reported using INT-767 (**1**) in animal models for the treatment of NASH [7] and NAFLD [8] conditions. Likewise, INT-767 (**1**) proved effective in diabetic nephropathy and retinopathy [9]. In addition to its efficacy against chronic cholangiopathies [10], it has also shown attenuation of intestinal ischemia reperfusion injury [11], reduction of hypercholesterolemia, visceral adipose tissue accumulation and development of atherosclerosis in rodent models [7,12–14].

A scalable synthesis to INT-767 (**1**) is thus needed to support the preclinical development and subsequent clinical trials. The retrosynthetic disconnection analysis for the synthesis of INT-767 (**1**) coalescing from OCA (**2**) involves as key steps the side chain shortening to

* Corresponding author. Laboratory of Medicinal and Advanced Synthetic Chemistry (LabMASC), Department of Pharmaceutical Sciences, Via del Liceo 1, 06123, Perugia, Italy.
E-mail address: antimo.gioiello@unipg.it (A. Gioiello).
[1] These authors contributed equally to the manuscript.
[2] Present address: Novartis Pharma AG, CH-4002 Basel (Switzerland).

https://doi.org/10.1016/j.ejmech.2022.114652
Received 15 June 2022; Received in revised form 27 July 2022; Accepted 31 July 2022
Available online 20 August 2022

the *nor*-intermediate and the final sulfation reaction of the primary alcohol (Fig. 1b). Extra-steps including protection/deprotection of the hydroxyl group at the steroidal body may be required to avoid side-products formation. In 2014, the target molecule **1** as its triethyl ammonium salt was described using the Beckmann reaction as key step starting from 6α-ethyl-7-keto-deoxycholic acid (**3**) in 9 steps and a 40% overall yield (Fig. 1c) [15].

In this work, we were challenged to develop a robust and scalable process for the preparation of pharmaceutical grade INT-767 (**1**). The strategy we pursued consisted in the evaluation of the diverse methods for the bile acid side chain degradation and the selective insertion of the sulfate group. The process was optimized using batch reaction screening utilized to identify potential bottlenecks that were addressed using greener approaches as the flow chemistry before attempting the scale-up. The optimized route has also been adapted for the synthesis of potential INT-767 metabolites that have been characterized and evaluated as agonists of FXR and TGR5 receptor.

2. Results and discussion

2.1. Side chain degradation

The degradation of the C24-carboxylic acid to the lower bile acid homologue can be achieved through four different strategies (Scheme 1): a) photochemical (tungsten lamp) decarboxylation in a CCl_4 solution of $Pb(OAc)_4$ and I_2 or of HgO and Br_2 [16], b) Beckmann rearrangement *via* mixed anhydride (TFAA) and nitrosation reaction with trifluoroacetyl nitrile (TFA, $NaNO_2$) [17], c) lead/copper-mediated oxidative decarboxylation ($Pb(OAc)_4$, $Cu(OAc)_2$) to the corresponding norcholene [18], or d) Barbier-Wieland degradation by Grignard addition (PhMgX), dehydration followed by oxidative cleavage [19]. All approaches when attempted on 5β-cholanoic acids evidenced several limitations, especially regarding scale-up operations. These include the use of hazardous reagents, requirement for extra protection and deprotection steps for the hydroxyl groups, long reaction times, and the need for extensive chromatographic purifications.

The Barbier-Wieland degradation route was selected as the strategy of choice. We initially focused on addressing the main challenges; indeed, previous procedures required anhydrous conditions, gave moderate to low yields of product, and required tedious chromatographic purifications. Importantly, despite these issues the reaction to obtain the *bis-nor*-5β-cholanyldiphenylethylene intermediate was scaled-up up to 100 g of deoxycholic ester as the starting material [19]. The experimental conditions involved the use of a large excess of phenylmagnesium bromide (17 eq.) in refluxing dry benzene to give the carbinol intermediate that was then acetylated and dehydrated in a refluxing solution of glacial acetic acid and acetic anhydride. The pure product was obtained in 74% yield and reacted with CrO_3 in a solution of glacial acetic acid, water, $CHCl_3$ at about 50 °C. The crude diacetate was then hydrolyzed in refluxing 10% aqueous KOH to furnish the *nor*-bile acid derivative in 69% yield [19]. Nowadays, diverse protocols are available for batch synthesis and although major advances have been made, further criteria need to be met for modern manufacturing processes.

Initially, we focused on avoiding the use of benzene and to reduce the number of equivalents of the Grignard reagent. THF was selected as the reaction solvent and the optimal amount of phenylmagnesium bromide was determined after performing screening experiments on the OCA methyl ester **3** (Table 1). The yield was determined by calibrated ^1H NMR analysis of the crude reaction mixture after acid-promoted (EtOH, HCl, 50 °C) dehydration of the carbinol intermediate. Starting from the conditions reported in the literature (17 eq. of PhMgBr in refluxing THF), the best balance between yield and reagent economy was obtained using 10 eq. of PhMgBr (Table 1, entry 2) while a further

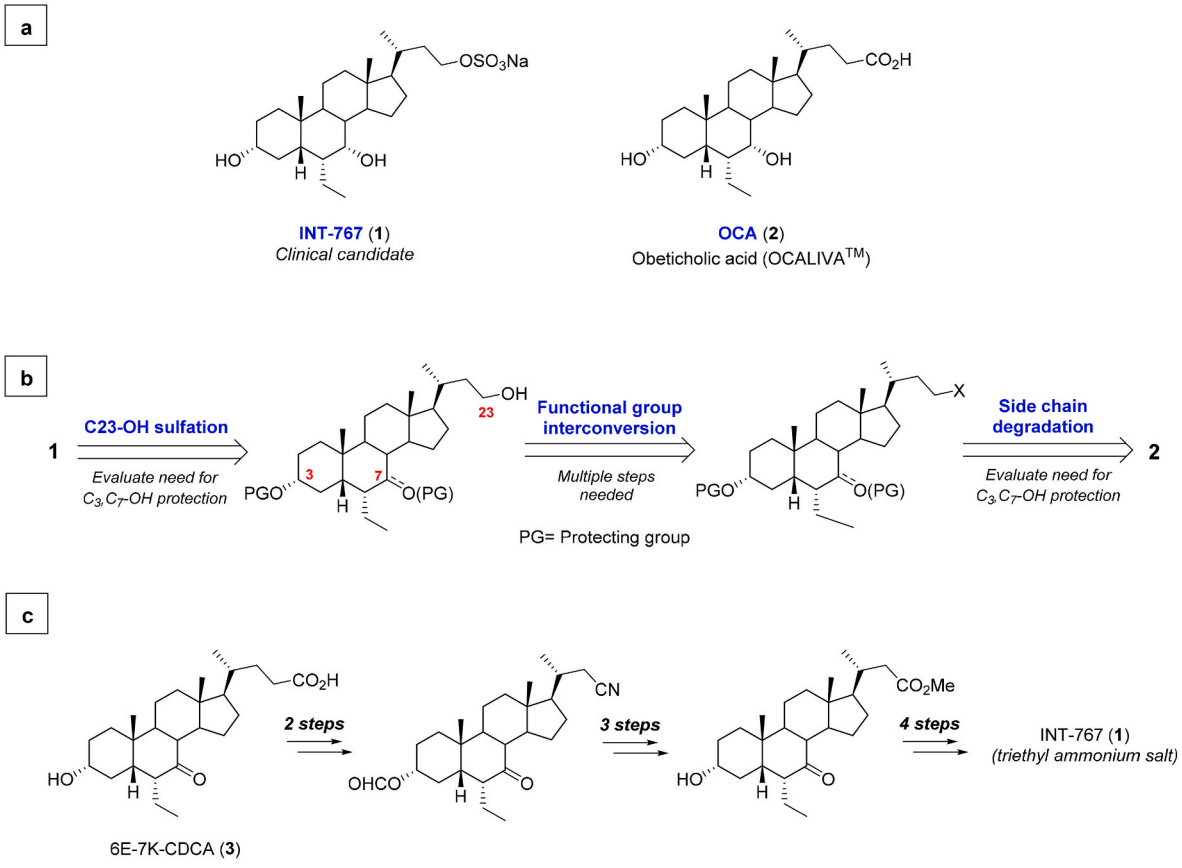

Fig. 1. a) Structure of INT-767 (**1**) and OCA (**2**). b) Retrosynthesis of INT-767 (**1**) from OCA (**2**). c) Previous synthetic approach to INT-767 (**1**) from 6E-7K-CDCA (**3**).

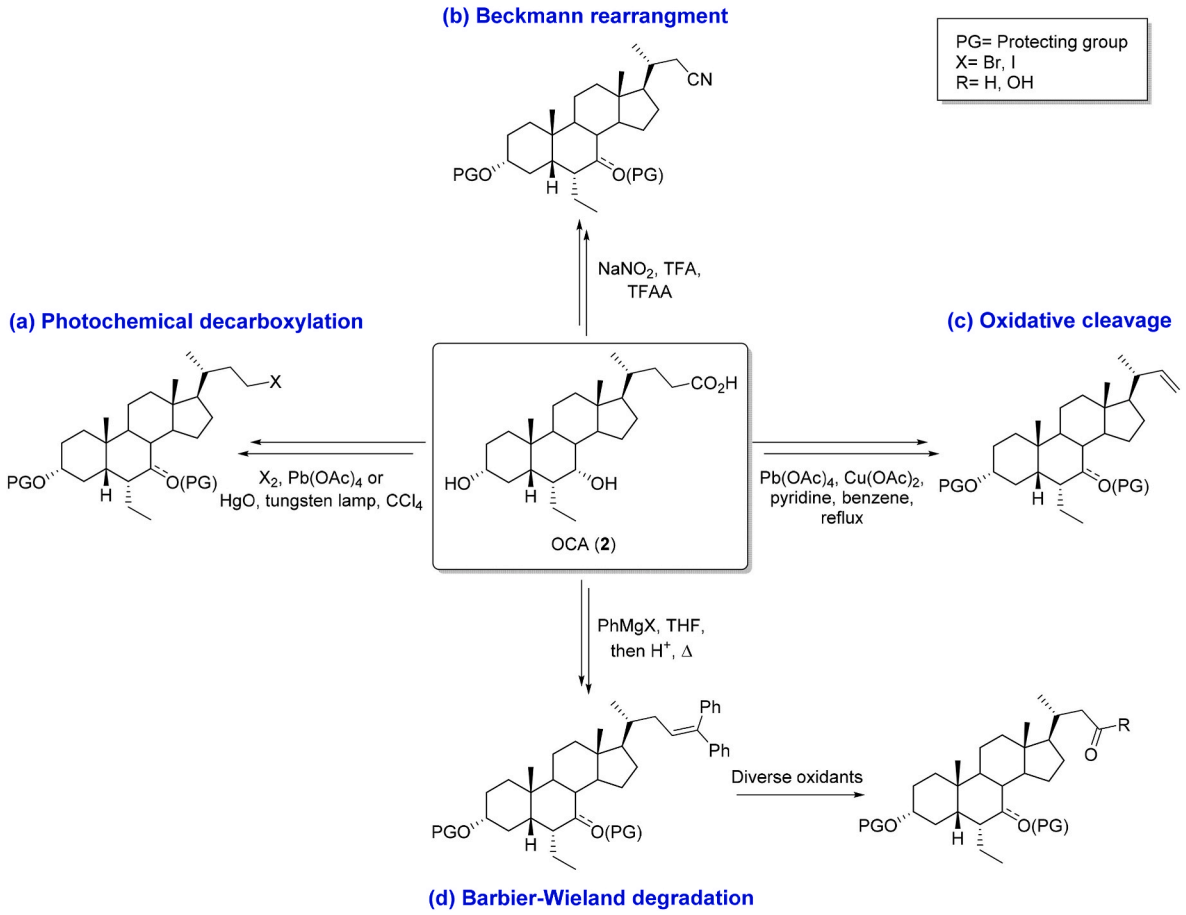

Scheme 1. Synthetic approaches for the degradation of the C24-carboxylic acid of bile acids. (a) photochemical decarboxylation, (b) Beckmann rearrangement, (c) Lead/copper-mediated oxidative decarboxylation, and (d) Barbier-Wieland degradation by Grignard reaction, dehydration, and oxidative cleavage.

Table 1
Evaluation of phenylmagnesium bromide equivalents.[a].-

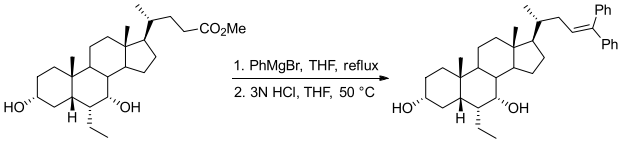

3 4a

entry	PhMgBr eq.	yield [b]
1	17	84%
2	10	80%
3	7.5	66%
4	5	50%
5	2.5	Traces

[a] Reactions were performed on 100 mg of **3** (0.23 mmol). *Reagents and conditions:* [**3**] = 0.1 M in THF, 3 M PhMgBr in Et_2O (2.5–17 eq.), reflux, o.n.; then 3 N aqueous HCl, EtOH, 50 °C, 4 h.

[b] Determined by calibrated ^1H NMR using dimethyl sulfone as the internal standard.

reduction of the Grignard reagent stoichiometry resulted in a progressive lowering of the reaction yield. Intermediate **4a** was then prepared at 10 g scale (80% isolated yield) for investigating the next oxidative cleavage step.

The oxidative cleavage of 24,24-diphenyl 3α,7α-dihydroxy-6α-ethyl-5β-cholan-23-ene (**4a**), also known as *bis-nor*-5β-cholanyldiphenylethylene, has previously been conducted by means of CrO_3 in a solution of glacial acetic acid, water, $CHCl_3$ at ~50 °C [19]. However, the use of CrO_3 is unsatisfactory given its toxicity, flammability and explosive limits [20]. To make this step more sustainable for large scale preparation, we elected to explore the potential of using flow ozonolysis chemistry. Despite several reported applications, most existing protocols possesses limitations, which affect their application in common laboratory practice and industrial processes [21]. However, the high versatility to a wide range of substrates is such that it is widely used. This is despite ozone being potentially dangerous, needing to be formed *in situ* as its storage is not possible, and the requirement for suitable production equipment, thus increasing overall costs. In this context, continuous flow technology can be particularly attractive as a valuable alternative to batch approaches to increase safety standards [22] and to facilitate the translation of hazardous chemical transformations including those involving gaseous reagents under elevated pressures [23–25]. Accordingly, several flow-based approaches and devices have been described in the literature able to realize ozonolysis reactions. Beyond safety considerations, the implementation of ozone as oxidizing agent avoids the need for extra-steps pertaining to the protection of the hydroxyl groups on the steroidal body.

Initially, the reaction was evaluated under batch conditions on both the free and protected intermediates **4a,b** (Scheme 2). Ozone was bubbled into a solution of **4a,b** in a mixture of CH_2Cl_2/MeOH (1:1 v/v, 0.12 M) cooled at −60 °C. After the complete conversion of the starting material, the reaction was quenched by adding triphenylphosphine to form the C24-*nor* aldehyde (**5a,b**) that was reduced by treatment with $NaBH_4$ in THF/H_2O. The desired C24-*nor* cholan-23-ol intermediates **6a** and **6b** were isolated in 70% and 65%, respectively, after silica gel flash chromatography (Scheme 2).

We next conducted the ozonolysis reaction under continuous flow

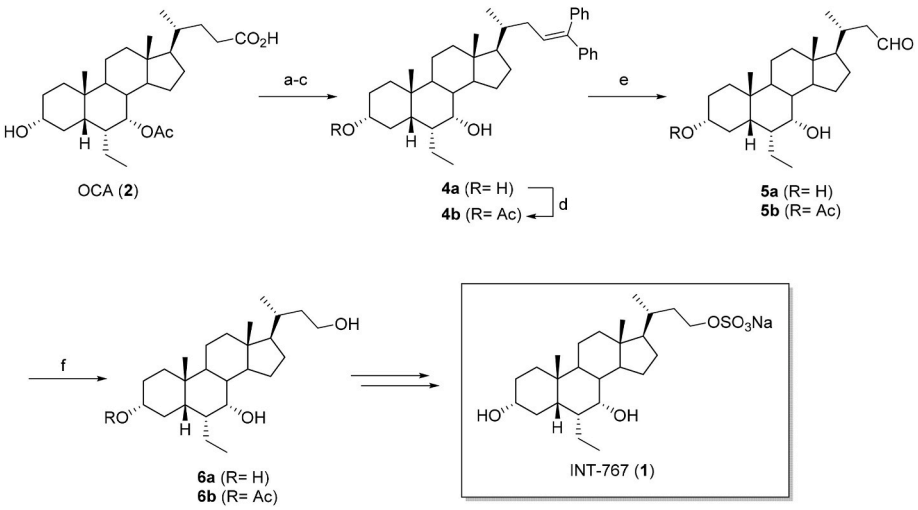

Scheme 2. *Reagents and conditions*: (a) *p*TSA, MeOH, ultrasound; (b) PhMgBr, THF, reflux, 25 °C; (c) HCl, EtOH, 50 °C, 80% from **2**; (d) Ac_2O, DMAP, pyridine, THF, 25 °C; (e) O_3, CH_2Cl_2, MeOH, −60 °C, then PPh_3; (f) $NaBH_4$, THF, H_2O, 0 °C → 25 °C, 70% from **4a** and 65% from **4b**.

conditions using a commercially available benchtop unit for ozone generation (Ozonia Triogen laboratory ozone generator) (Scheme 3) [26,27]. Continuous flow technology can provide many advantages over traditional batch synthesis [28–30]. In the case of gas-liquid reactions, the use of continuous flow reactors has facilitated access to transformations that were deemed to be either too dangerous to be conducted at large scales in batch or not efficient due to the contact time of high-pressure requirements of the gases [31]. Thus, the ozone stream generated from molecular oxygen contained into a pressurized reservoir, was mixed at 1 L min^{-1} with a 0.12 M stock solution of **4a,b** in CH_2Cl_2/MeOH (1:1, v/v) pumped by a HPLC pump at 1 mL min^{-1}. The resulting liquid-gas biphasic system was flowed through a reactor coil (I. D. x O.D. = 1.6 mm × 3.2 mm, 50 mL) cooled at 0 °C (τ = 6 min). The output was collected into a round bottom flask in the presence of a stirring solution of $NaBH_4$ (4 eq.) in MeOH at 25 °C enabling both the quenching of ozone and the reduction of the C23-aldehyde group into the corresponding alcohol (**6a,b**) in excellent yields (88–90%) (Scheme 3). Remarkably, the ozonolysis reaction did not involve any competitive oxidation reaction at either the C3 or C7 positions ruling out the need of C3–OH protection. This represents a great advantage to streamline the

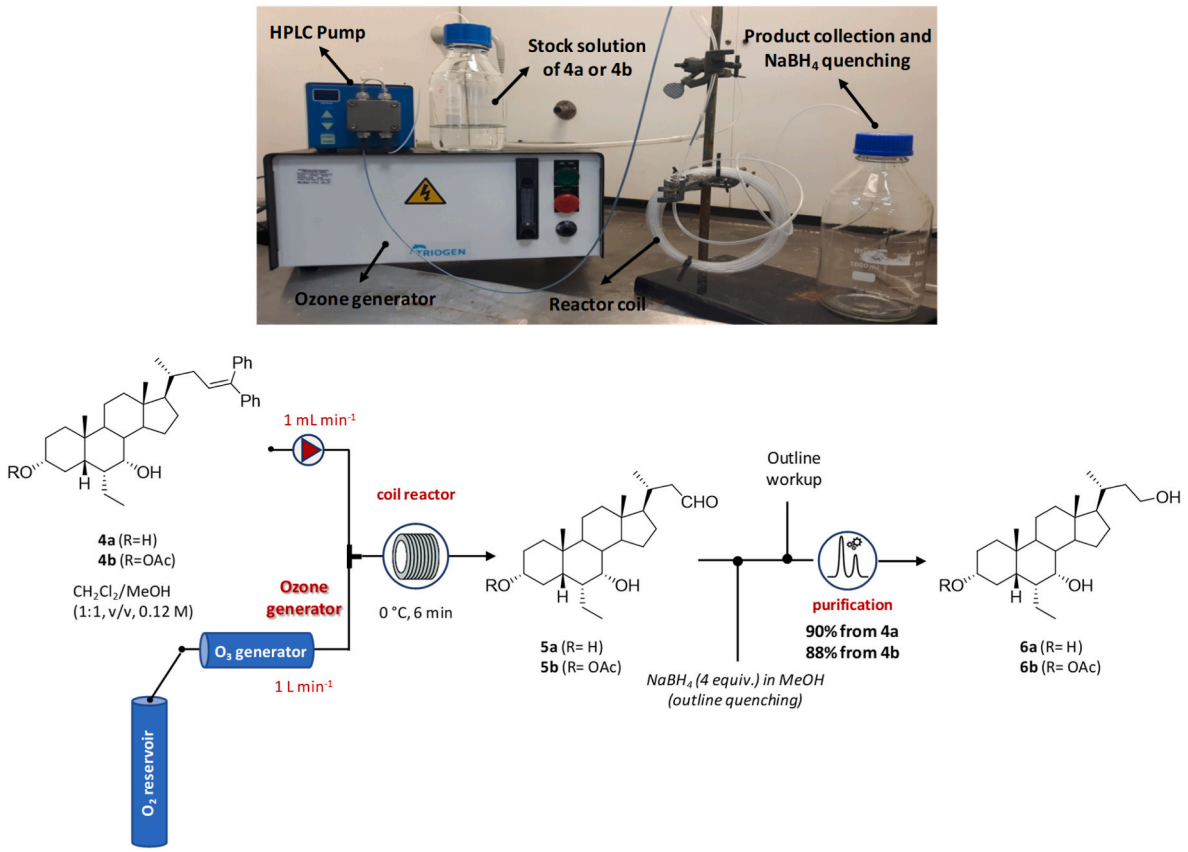

Scheme 3. Flow set-up and equipment for the one-pot two-step oxidative cleavage to C24-*nor* derivative **6a,b**.

overall process as we observed that the triol intermediate **6a** can easily crystallize from *tert*-butyl methyl ether facilitating the purification and avoiding time-consuming and expensive chromatography.

2.2. Sulfation reaction

The selective formation of sulfate groups remains a challenging synthetic aspect [32]. The presence of one or more hydroxyl groups makes chemical synthesis and purification of (per)sulfated compounds difficult, primarily due to their poor solubility in organic solvents. Our primary goal was to obtain the regioselective sulfation of the primary alcohol at the C23 position over the hydroxyl groups on the steroidal body. While a certain selectivity could be expected for the C7–OH group, which is sterically hindered, the C3–OH of bile acids has often shown a similar reactivity to the side chain primary alcohol. Among the wide variety of methods to prepare organosulfates [33], the use of sulfur trioxide amine/amide complexes and sulfuryl imidazolium salts were more suitable than others for our purpose. The complexes are relatively easy to prepare and are stable at high temperatures. We initially considered the possibility of employing the N, N′-dicyclohexylcarbodiimide (DCC)-sulfuric acid at different temperature (see Table S1, Supplementary material). Thus, compound **6a** was reacted with DCC (5 eq.) in DMF at either 0 or -45 °C and then with a DMF solution of H_2SO_4 (1 eq.). Under these conditions we observed the formation of an equimolar mixture of the desired C23-monosulfate **1**, C3-monosulfate and the C3,C23-disulfate evidencing a low regioselectivity (conversion yield: 50%) (see Table S1, Supplementary material). Based upon this outcome we next investigated a range of amine-sulfur trioxide complexes including N-ethylmorpholine-sulfur trioxide complex, N,N-diisopropylethylamine-sulfur trioxide complex, and sulfur trioxide-pyridine complex [34]. The reactions were performed by dropwise addition of the amine-sulfur trioxide complexes (1.05 eq.) to a solution of triol **6a** in CH_2Cl_2. Unfortunately, none of amine-sulfur trioxide complexes gave satisfactory results in terms of both yield and selectivity (see Table S2, Supplementary material). The use of the flow chemistry was also investigated by means of polymer-supported pyridine-sulfur trioxide complex packed in a column reactor. Reactions were performed by pumping a stock solution of the triol **6a** (0.3 M in DMF or 0.25 M in pyridine) through a pre-packed column (at 5 μL min^{-1}; τ = 47 min) filled with the polymer-supported pyridine-SO_3 complex (1.05 or 10 eq.) heated at different temperature (25 °C, 40 °C or 60 °C) (Scheme 4). Again, we failed to obtain the desired products **1** in a regioselective manner (see Tables S1–2, Supplementary material). These outcomes forced us to conduct the sulfation reaction on the C3-protected C24-*nor* intermediate **6b**. Thus, compound **6b** was dissolved in dry pyridine and treated with pyridine sulfur trioxide complex (pyr·SO_3) (1.3 eq.) at 25 °C. Finally, the crude reaction mixture was submitted to alkaline hydrolysis (NaOH/MeOH) under reflux to furnish INT-767 (**1**) in 78% yield after C18 reverse phase chromatography.

2.3. Integrating flow and batch chemistry

A synthetic route that integrates batch and flow chemistry for the multigram preparation of INT-767 (**1**) is depicted in Scheme 5. Thus, methyl ester **3** (10 g) was submitted to the Barbier Wieland degradation in THF using 10 eq. of PhMgBr. After acid-promoted dehydration (HCl/MeOH, 50 °C), intermediate **4a** was obtained in 80% isolated yield. The C3–OH was then protected using acetic anhydride, pyridine, DMAP in THF at 25 °C. Ozonolysis of the olefin derivative **4b** was successfully scaled-up in flow. Specifically, a telescoped one-pot two-step procedure was performed in a continuous mode without solvent switch using a readily assembled flow ozonolysis device, as previously discussed. After a standard workup procedure to quench $NaBH_4$, the crudes were collected and purified by automated flash chromatography affording the corresponding C24-*nor* alcohol derivatives **6b** in 88% isolated yield from **4b** on multigram scale (Scheme 5). The final sulfation step was performed on the C3-acetylated intermediate **6b** using pyr-SO_3 in pyridine. The acetyl group was finally removed by treatment with NaOH in MeOH and the desired INT-767 (**1**) was obtained in 78% yield from **6b** and in 55% overall yield over 7 steps from OCA (**2**) (Scheme 5).

2.4. Synthesis, characterization and SAR of INT-767 metabolites

Drug metabolism is an important component in drug development and the effects of drug metabolism on pharmacokinetics (PK), pharmacodynamics (PD), and safety need to be carefully considered [35]. It is therefore of paramount importance to evaluate the toxicity and activity of metabolites and perform adequate drug bioavailability, PK and PD studies. Toward this end, we designed and synthesized putative INT-767 metabolites **6a, 7–9** (Fig. 2) for future drug investigations. The metabolism of natural and semi-synthetic bile acids is indeed a complex set of enzymatic reactions that occurs during the enterohepatic circulation [36–38].

Bile fistula rat experiments showed that INT-767 (**1**) is mainly converted into the 3-glucuronide metabolite (**7**) [6]. The glucuronidation process is a common metabolic pathway in humans and plays an important role in liver pathology (e.g. cholestasis) [39]. The oxidation of the hydroxyl group at the C3 position of the bile acid nucleus is catalysed by the enzyme 3α-hydroxysteroid dehydrogenase (3α-HSD) [40]. In the liver, the interconversion between 3α-hydroxy and 3-keto facilitates the transit of bile salts from the sinusoidal to the canalicular side of the hepatocytes. Triol **6a** can be formed in vivo by the action of microbial bile salt desulfatase in the intestine, as well documented in the literature [41]. Alternatively, sulfatases may be involved in the formation of sulfate metabolites as compound **8**, which is generally formed in cholestatic patients as a detoxification pathway [42].

2.4.1. Synthesis

The synthesis of INT-767 3β-D-glucuronide disodium salt (**7**) was achieved by a Koenigs-Knorr reaction [43]. Thus, INT-767 (**1**) was dissolved in anhydrous toluene and treated with methyl 2,3,4-tri--O-acetyl-α-D-glucopyranosyluronate bromide (**10**) in the presence of

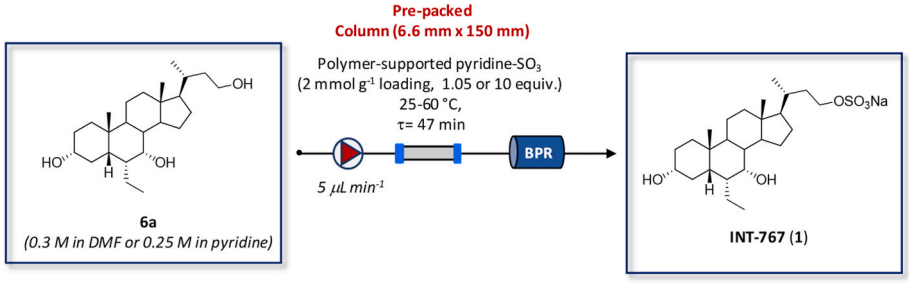

Scheme 4. Flow set-up used for the attempted selective sulfation reaction of the primary alcohol.

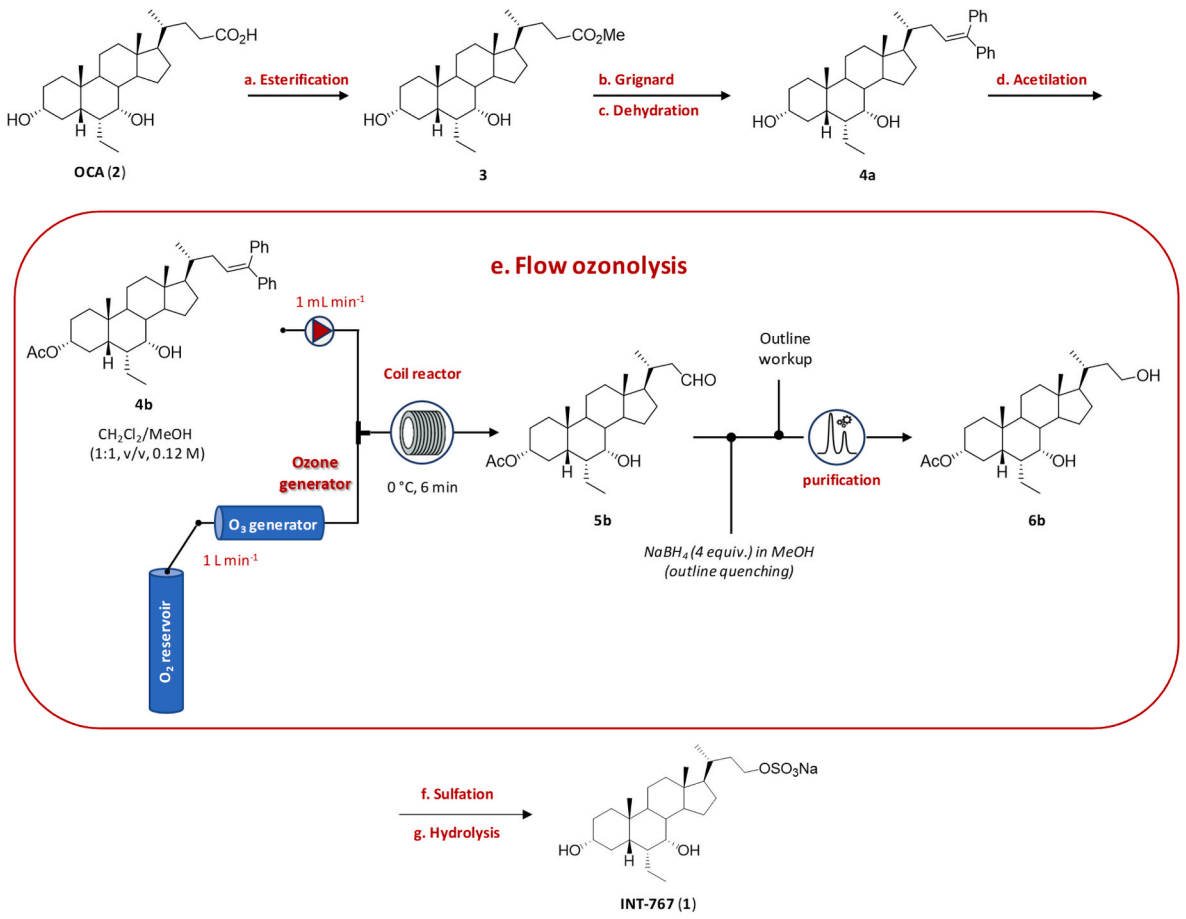

Scheme 5. Integrated batch and flow approach for the synthesis of INT-767 (1). Reagents and conditions: (a) MeOH, pTSA. H_2O, u.s.; (b) PhMgBr, THF, reflux; (c) HCl, EtOH, 50 °C, 80% from 2; (d) Ac_2O, pyridine, DMAP, THF, 25 °C; (e) O_3 stream, 0 °C, $\tau = 47$ min; then $NaBH_4$, MeOH, 88% from 4a; (f) Pyr·SO_3, pyridine, 25 °C; (g) NaOH, MeOH, reflux, 78% from 6b. Overall yield: 55%.

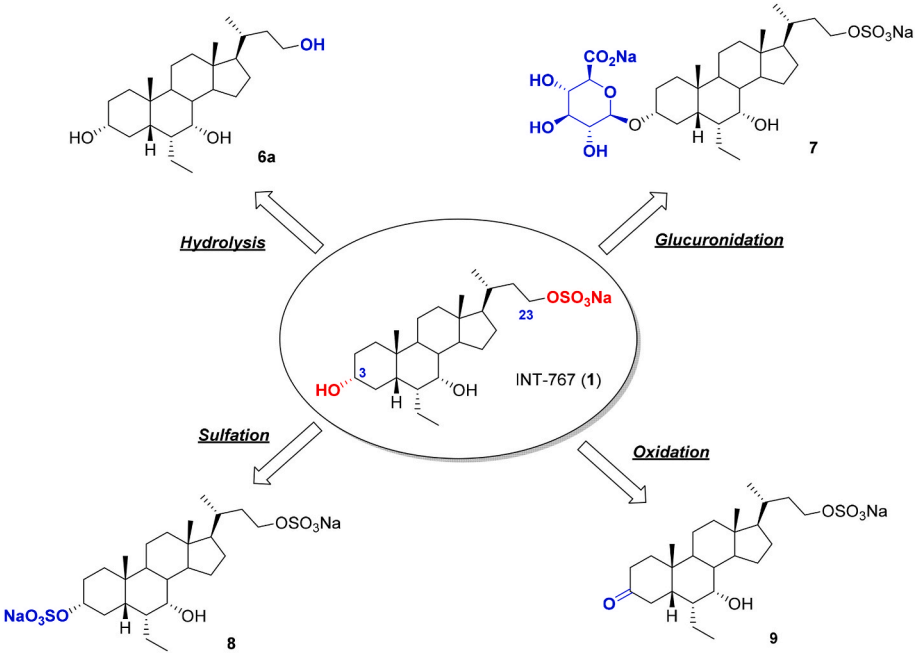

Fig. 2. Potential metabolites expected in vivo from INT-767 (**1**). Metabolic hot-spots of INT-767 (**1**) are shown in red while the functional groups of the metabolites are in blue.

Fetizon's reagent and molecular sieves under dark conditions. The corresponding 3β-D-glucuronide methyl ester-triacetate derivative **11** (78% isolated yield) was subjected to alkaline hydrolysis under mild conditions to give the desired INT-767 3β-D-glucuronide disodium salt (**7**) in 92% isolated yield after RP-18 chromatography (Scheme 6). The synthesis of the corresponding 3-oxo derivative **9** started from the reaction of **1** with Ac_2O and $Bi(OTf)_3$ at 25 °C, followed by regioselective hydrolysis of the acetyl group at C3 position (Scheme 6). The thus formed 7α-acetoxy derivative **12**, obtained in 85% yield after silica purification, was treated with Dess-Martin periodinane in CH_2Cl_2 and alkaline hydrolysis to give the desired 3-oxo INT-767 analogue **9**, in 41% yield over 4 steps. Finally, sulfation of **1** with pyr·SO_3 (3 eq.), pyridine afforded the disulfate **8,** in 61% yield (Scheme 6).

2.4.2. FXR and TGR5 activity

The newly prepared metabolites (**6a**, **7–9**) were tested in a biochemical AlphaScreen assays and HTR-FRET to evaluate their ability to activate FXR and TGR5 receptors, using chenodeoxycholic acid (CDCA) and litocholic acid (LCA) as the reference standards, respectively. As reported in Table 2, all the metabolites resulted less active than INT-767 (**1**) confirming the importance of the sulfate moiety at C23 position and the hydroxyl group at C3α position as key structural features for the activation of both receptors.

Except compound **8**, the screened metabolites retained FXR agonistic activity and exerted a full agonistic profile. Triol **6a** retained a dual FXR/TGR5 full agonistic profile in the micromolar range of potency suggesting that the removal of the sulfate moiety at C23 position is detrimental for binding affinity but it is still accepted for the receptor activation. Moreover, persulfatation at the C3 position resulted in a loss of activity at both receptors. Interestingly, like the 3-oxo-CDCA that maintained a similar FXR potency as the parent CDCA [44], compound **9** was a nanomolar FXR agonist albeit three times less active than INT-767 (**1**) (FXR EC_{50} = 0.08 vs 0.03 μM, respectively). Similarly, a loss of affinity was observed towards the TGR5 receptor. Finally, the presence of the glucuronic unit induced the loss of TGR5 activity while maintaining a full FXR agonism in the micromolar range of potency.

Table 2
Biological characterization of INT-767 metabolites **6a**, **7–9** as FXR and TGR5 ligands.[a]

Compound	hFXR[b] (AlphaScreen Assay)		hTGR5[c] (HTR-FRET)	
	EC_{50} (μM)	Efficacy (%)	EC_{50} (μM)	Efficacy (%)[d]
INT-767 (**1**)	0.030 ± 0.005	280 ± 5	0.68 ± 3	120 ± 5
OCA (**2**)	0.15 ± 0.5	230 ± 10	14 ± 2	52 ± 4.4
INT-777 (**13**)	>100	n.d.	0.9 ± 0.03	117 ± 2
7	5 ± 0.4	115 ± 5	>100	n.d.
9	0.08 ± 0.02	162 ± 3	5 ± 1	98 ± 2
6a	1.2 ± 0.2	165 ± 40	1.1 ± 0.2	117 ± 2
8	>100	n.d.	>100	n.d.

[a] Data represent mean values ± SD of at least three independent experiments.
[b] Units are μM for EC_{50} and % of 50 μM CDCA value for efficacy.
[c] Units are μM for EC_{50} and % of 10 μM LCA value for efficacy.
[d] Efficacy values are here used as a measure of fluorescence change. n.d.: not determined.

2.4.3. Molecular docking into FXR

The binding modes of INT-767 (**1**), its metabolites (**6a**, **7–9**) and OCA (**2**) into FXR were investigated using molecular docking and the available crystal structure of the active conformation of the receptor ligand binding domain (LBD) as obtained from the co-crystallization studies with compound **2** (PDB code 1OSV) [44]. Table 3 reports the top scoring

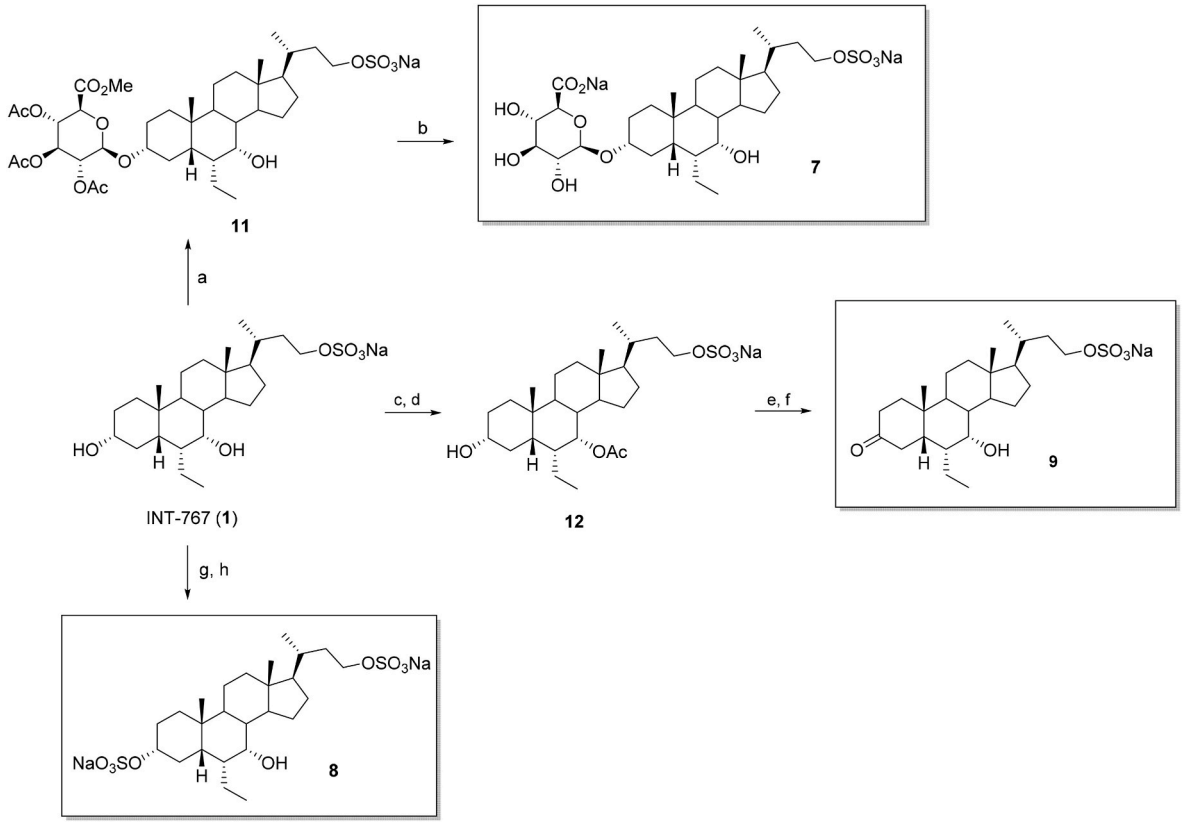

Scheme 6. Synthesis of INT-767 metabolites (7–9). Reagents and conditions: (a) Methyl 2,3,4-tri-O-acetyl-α-D-glucopyranosyluronate bromide (10) (3 eq.), Fetizon's reagent (10 eq.), toluene, 25 °C, dark conditions, 78%; (b) Na_2CO_3 (20 eq.), MeOH, 25 °C, 92%; (c) Ac_2O (10 eq.), $Bi(OTf)_3$ (0.05 eq.), CH_2Cl_2, 25 °C; (d) NaOH (3 eq.), MeOH, 25 °C, 85% from INT-767 (1); (e) Dess-Martin periodinane (3 eq.), CH_2Cl_2, 25 °C, 18 h; (f) NaOH (20%, wt), MeOH, reflux, 48% from 12. (g) pyr·SO_3 (3 eq.), pyridine, 25 °C; (h) NaOH, MeOH/H_2O, 25 °C, 61% yield from INT-767 (1).

Table 3
Scored binding mode at FXR.

Ligand	FXR	1OSV Chain A			1OSV Chain B		
	pEC_{50} (μM)	Gscore SP (kcal/mol)	Emodel (kcal/mol)	MMGBSA ΔG (kcal/mol)	Gscore SP (kcal/mol)	Emodel (kcal/mol)	MMGBSA ΔG (kcal/mol)
INT-767 (**1**)	3.51	−11.60	−94.13	−90.37	−11.36	−91.40	−79.27
OCA (**2**)	1.90	−11.95	−95.14	−89.68	−12.14	−106.77	−78.61
6a	−0.18	−11.79	−86.66	−102.71	−11.35	−86.18	−87.49
8	−4.61	−9.46	−45.43	−65.67	n.d.	n.d	n.d.
7	−1.61	n.d.	n.d.	n.d.	n.d.	n.d	n.d.
9	2.53	−11.80	−97.05	−98.92	−10.68	−90.40	−92.94

binding modes of these compounds when docked into the chain A and B of the crystal structure 1OSV. In particular, the ligand binding energy of each solution was evaluated using the Gscore standard precision (SP) function, the Emodel score for pose selection, and the molecular mechanics-generalized Born surface area (MMGBSA) method.

A poor correlation was found between the calculated ligand binding energies of the top scoring solutions and the coactivator recruitment activity of compounds in the FXR AlphaScreen assay, expressed as pEC_{50} (-ln EC_{50}). This observation suggests that the adopted scoring functions (Gscore SP, Emodel, MMGBSA) are unable to provide a correct estimation of the binding energy of these compounds to the LBD of FXR. Moreover, different binding energies of the top scored solutions are obtained when docking ligands into chain A and chain B of the crystal structure 1OSV. At odds with these discrepancies, the calculated binding mode of OCA, when docked into chain A and B of the cognate crystal structure (top scoring solution), shows a very good agreement with the experimental binding mode in both chains of 1OSV (root mean square deviation, RMSD< 0.5 Å see Fig. S1, Supplementary material). Hence, the presence of subtle conformational differences between the ligand binding clefts of chain A and chain B determines different estimations of the ligand binding energy and may affect the calculation of the ligand binding mode to the receptor, as observed in the case of compounds **7** and **8**. Specifically, the overlap between chain A and B of 1OSV reveals different conformations of the loop region (residues 259–262) connecting helix H1 to helix H2 (see Fig. S2, Supplementary material). In turn, these conformations generate different shapes of the ligand binding cleft, with chain A showing a larger cavity than chain B. Consequently, the narrow binding cleft of chain B is not suitable to study the binding mode of active compounds larger than OCA (**1**), such as compound **7**, whereas chain A is more permissive, yet sterically demanding for the larger compound **7**.

To gain insights into the structure-activity relationships, we next analyzed the top scoring solutions of active compounds **1**, **2**, **6a** and **9** into chain B of 1OSV. Given the lack of reliability of the adopted scoring functions (Gscore SP, Emodel, MMGBSA), surfaces representing interaction property complementarity (Fig. 3) and a qualitative assessment of interactions between binding site residues and docked ligands (Fig. 4) were considered, rather than ligand binding energies. Fig. 3 reveals that the ligand binding site of FXR is endowed with a large central hydrophobic core (Hy) that accommodates the steroid nucleus and the C6α ethyl group of the bile acid derivatives. Two hydrogen bond donor pockets (P1: Tyr358, His444; P2: Arg328) surround the terminal aspects of the ligand at C3α and C23/C24 positions, respectively, whereas two additional hydrogen bond acceptor pockets are located nearby position C7α (P3: Ser329; P4: Tyr366). Although all compounds share the same interactions in pockets P3 and P4, making hydrogen bonds between the conserved C7α hydroxyl group and the side chain of Ser329 or Tyr366, different interactions occur at P1 and P2 (Fig. 4). Specifically, the pocket of the receptor accomodating the terminal C23/C24 acidic group (P2) bears a neutral formal charge, since Arg328 is involved in a salt bridge interaction with Glu331.

As previously reported [45], such structural peculiarity allows for an atypical replacement of the carboxylic group with a primary amine moiety in bile acids that maintain the FXR agonist activity [46]. Thus,

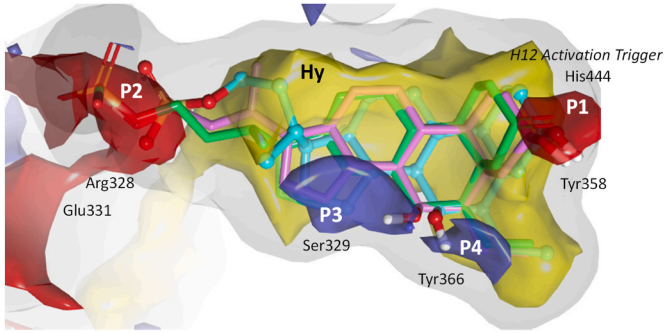

Fig. 3. Surfaces representing interaction property complementarity of FXR binding site (chain B 1OSV) mapped on the overlay of top scored solutions from the docking study of compounds **1**, **2**, **6a** and **9**. Yellow surface shows the hydrophobic pocket of the receptor (Hy); red surfaces show hydrogen bond donor areas (P1: Tyr358, His444; P2: Arg328); purple surfaces show hydrogen bond acceptor areas (P3: Ser329; P4: Tyr366). The image was generated using SiteMap.

the higher activity of INT-767 (**1**) than OCA (**2**) can be tentatively explained with the reported observation that sulfate groups, on a statistical basis, preferentially occupy polar binding sites bearing a neutral formal charge [47]. In such a neutrally charged local environment, the sulfate group would make stronger hydrogen bond interactions than the analogous carboxylic group (Fig. 7a and b) whose intensity is not correctly estimated by the adopted scoring functions. In accordance with this observation, compound **6a,** in which the carboxylic group is replaced by the hydroxyl group, still retains the FXR agonist activity in the low micromolar range of potency, albeit with one-fold lower potency than OCA (**2**) due to the presence of only one hydrogen bond interaction with Arg328 (Fig. 4c). The other terminal hydrogen bond donor pocket (P1: Tyr358, His444) is located nearby the activation function of the nuclear receptor (helix H12), and contains two residues of the triad (Tyr358, His444, Trp466) whose conformational changes and hydrogen bond interactions account for the recruitment of the coactivator. In contrast to pocket P2 (Arg328), pocket P1 is more demanding in terms of steric and hydrogen bond properties of the functional group inserted at C3 position of the bile acid scaffold. Indeed, compounds **1**, **2** and **6a** can make two hydrogen bond interactions with Tyr358 and His444, the first being a donor type and the second an acceptor type (Fig. 4a–c). The lack of this dual faced hydrogen bonding property at the C3 position determines a decrease of coactivator recruitment efficacy in compound **9** (Fig. 7d).

Docking studies of compound **8** return a solution only when using chain A of 1OSV with a larger binding site as template structure. On the basis of such solution, the lack of recruitment activity for compound **8** in the FXR AlphaScreen assay (Table 2) may again be explained with the lack of the hydrogen bond donor complementarity of the sulfate group at C3 to engage the side chain of Tyr358 (see Fig. S3, Supplementary material). Although a reliable docking solution for compound **7** into chain A or B of 1OSV is lacking, it is envisaged that this compound might adopt a similar binding pose to OCA (**2**), with the hydroxyl groups of the

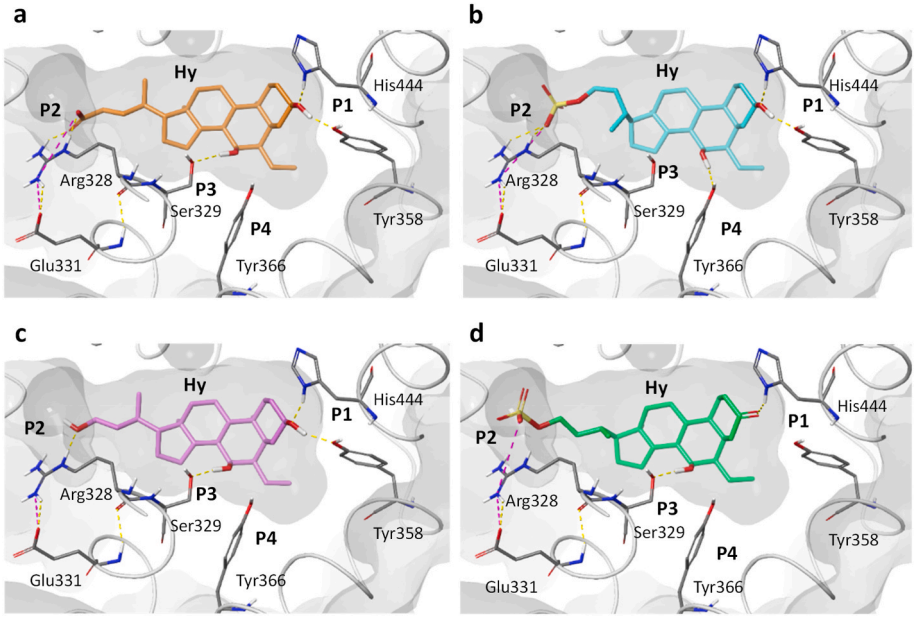

Fig. 4. Top scored solutions from the docking study into chain B 1OSV of OCA (a), INT-767 (b), compounds **6a** (c) and **9** (d). Hydrogen bond interactions are shown with yellow dashed lines. Ionic interactions are shown with purple dashed lines. Interacting residues are labelled. The images were generated with the software Maestro, using chain B of 1OSV after its processing with the Protein Preparation Wizard (PPW) tool.

glucuronic moiety making acceptor and donor hydorgen bonds with Tyr358 and His444 while region P1 undergoes significant conformational changes to accommodate this bulky moiety.

2.4.4. *Molecular docking into TGR5*

The recent cryo-electron microscopy (EM) structure of TGR5 (PDB code 7CFN) in complex with INT-777 (**13**) [46] was used to study the binding mode of INT-767 (**1**), its metabolites (**6a**, **7–9**) and OCA (**2**) into the seven transmembrane helical receptor. Although a poor correlation is still observed between the calculated ligand binding energies of the top scored solutions and the agonist activity of compounds (-ln EC_{50}) in the TGR5 cellular assay (Table 4), a low agreement is found between the calculated binding mode of INT-777 (top scored solution) and its experimental binding mode in 7CFN (root mean square deviation, RMSD = 1.5 Å, Fig. 5), with the largest displacement being observed on the side chain atoms of the compound.

Given the poor reliability of the adopted scoring functions (Gscore SP, Emodel, MMGBSA), as discussed in the case of FXR, structure-activity relationships were analyzed inspecting surfaces representing interaction property complementarity and the interactions of active compounds (**1–2**, **13**, **6a** and **9**) into 7CFN, according to the top scoring solution. In contrast to the FXR binding site (Fig. 3), the surface mapping of TGR5 binding site reveals more pockets of potential ligand interactions (P1–P6) beside the central hydrophobic pocket (Hy) accommodating bile acids' steroid nucleus (Fig. 6). Specifically, two pockets for hydrogen bond donor interactions (P1: Tyr240; P2: Tyr89, Ala250, Gln253) are located at C3 and C23/C24 positions, respectively. Likewise, four pockets for hydrogen bond acceptor interactions are located at C7 (P3: Ser247), C12 (P4: carbonyl group of Leu71), C16 (P5: Ser157) and C3 (P6: Ser270). According to the top score solutions (Fig. 7b–f), docked compounds make conserved hydrogen bond interactions between the C3α hydroxyl group (**1**–**2**, **7** and **13**) or C3 carbonyl group (**9**) and the side chain of Tyr240 (P1). Then, the carboxylic group (**2**, **13**) and the sulfate group (**1**, **9**) engage Tyr89 (P2) in a further hydrogen bond interaction, whereas the C23 hydoxyl group of compound **6a** is hydrogen bonded to the carbonyl group of Ala250 (P2). It is worth noting that, according to the experimental binding mode of INT-777 (**13**) in 7CFN, the side chain of this compound adopts a different conformation wherein the carboxylic group does not interact with any polar residue of the receptor (Fig. 7a). This observation provides an explanation to the low agreement found between the calculated binding mode and the experimental binding mode of INT-777 (**13**) (RMSD = 1.5 Å, Fig. 6), perhaps suggesting a poor energetic refinement of the EM structure of TGR5.

Table 4
Scored binding mode at TGR5.

Ligand	TGR5	7CFN		
	pEC_{50} (μM)	Gscore SP (kcal/mol)	Emodel (kcal/mol)	MMGBSA ΔG (kcal/mol)
1	0.39	−8.49	−69.93	−61.14
2	−2.64	−8.45	−70.38	−60.66
13	0.11	−8.42	−73.00	−64.96
6a	−0.10	−8.18	−61.35	−68.05
8	n.a.	−6.84	−54.71	−46.18
7	−4.61	−8.65	−48.21	−63.74
9	−1.61	−8.30	−68.22	−62.49

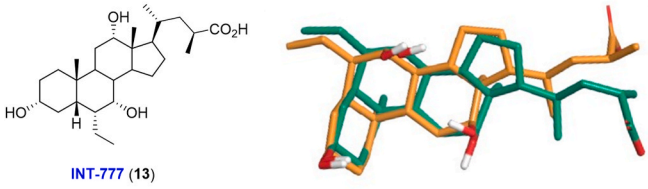

Fig. 5. Overlap between the experimental bioactive conformation (green carbon sticks) and the docked conformation of INT-777 (**13**) (orange carbon sticks) in 7CFN.

No clear interactions are observed engaging the C12α hydroxyl group of INT-777 (**13**), with the carbonyl group of Leu71 (P4) being the closest hydrogen bond acceptor group to such steroidal position (Fig. 7a and b). Conversely, a hydrogen bond interaction is observed between the C12α hydroxyl group of all compounds and the side chain of Ser247 (P3).

Consistent with the importance of these residues in the interaction with bile acids, mutagenesis experiments have shown that mutants

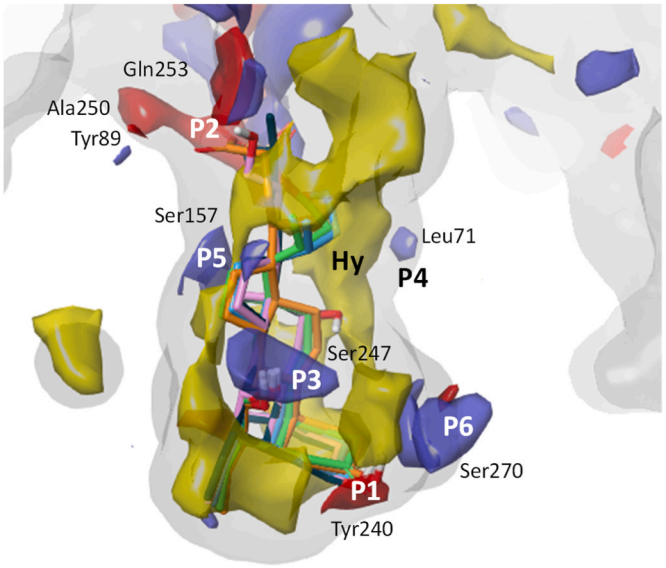

Fig. 6. Surfaces representing interaction property complementarity of TGR5 binding site (7CFN) mapped on the overlay of top scored solutions from the docking study of compounds **1**, **2**, **13**, **6a** and **9**. Yellow surface shows the hydrophobic pocket of the receptor (Hy); red surfaces show hydrogen bond donor areas (P1: Tyr240; P2: Tyr89, Ala250, Gln253); purple surfaces show hydrogen bond acceptor areas (P3: Ser247; P4: Leu71; P5: Ser157; P6: Ser270). The image was generated using SiteMap.

Tyr240Ala, Ser247Ala and Tyr89Ala impair TGR5 activation [48–50], whereas the significance of some other pockets of the binding site, such as P4 (carbonyl group of Leu71) and P5 (Ser157), have been highlighted through previous ligand-based computational studies [51,52]. The lack of TGR5 activity for compounds **7** and **8** can likely be ascribed to the presence of an unfavorable negative electrostatic environment at the bottom of the binding site, generated by Glu169, that is not complementary to the electrostatic potential distribution on the surface of these compounds showing extensive negative charged regions (see Fig. S4, Supplementary material).

3. Conclusions

In summary, we have described the synthesis development for the large scale preparation of INT-767 (**1**) [53], a bile sulfate submitted to clinical studies. Our approach reduces the step counts and overcomes previous synthesis limitations like the use of harsh reaction conditions and toxic reagents. Overall, our route leads to higher efficiency and yields under mild reaction conditions, the use of lower amount of reagents, simple downstream procedures, resulting in high quality material and improved safety standards, as well as in reduced costs and wastes.

In addition to ensuring ready availability of compound useful for advancing preclinical and clinical studies, we have prepared a series of INT-767 metabolites suitable for PD/PK studies. Moreover, the in vitro profile of such metabolites has shown a reduced potency at both FXR and TGR5 receptor with respect to the parent compound, as also confirmed by computational analysis. Molecular docking studies into

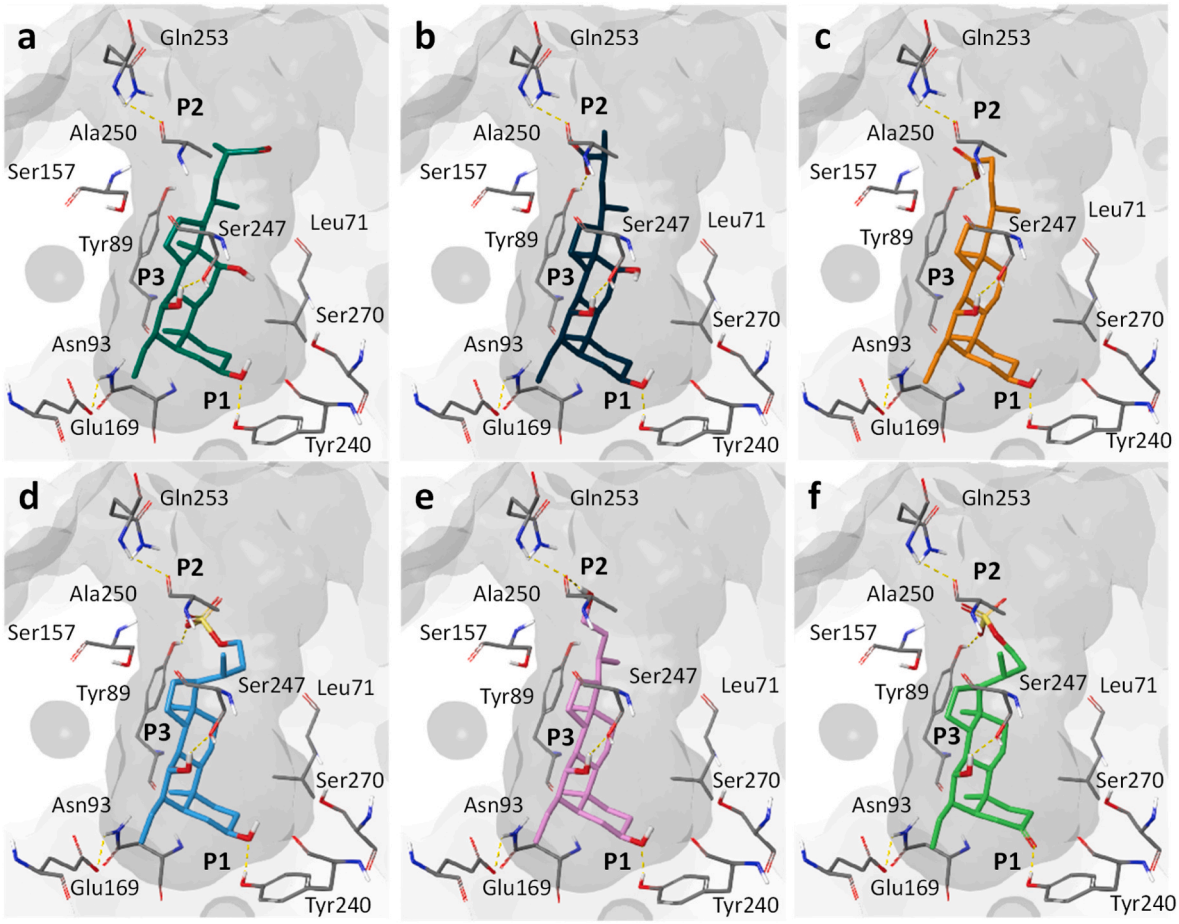

Fig. 7. Experimental binding mode of INT-777 (**13**) into 7CFN (a) and top scored solutions from the docking study of INT-777 (b), OCA (c), INT-767 (d), compounds **6a** (e) and **9** (f). Hydrogen bond interactions are shown with yellow dashed lines. Key residues surrounding the ligand are labelled. The images were generated with the software Maestro, using 7CFN after its processing with the Protein Preparation Wizard (PPW) tool.

the binding sites of FXR and TGR5 provide interesting insights into the structure-activity relationships of active compounds, including INT-767 (**1**) and some of its metabolites (**6a**, **9**). These models highlight the importance of the hydrogen bond complementarity at C3α of the bile acid scaffold with the side chains of residues Tyr358 and His444 for the coactivator recruitment activity in FXR, and the need of high electrostatic potential complementarity between bile acids and binding site residues for TGR5 activity.

4. Materials and methods

4.1. Chemistry

4.1.1. General methods

Unless otherwise noted, chemicals were obtained from commercial suppliers and used without further purification. Reactions requiring anhydrous conditions were conducted in flame-dried glass apparatus under a positive pressure of N_2 using freshly distilled solvent according to reported procedures. NMR spectra were recorded on a Bruker AC 400-MHz spectrometer (Bruker, Madison, WI, USA) in the indicated solvent. Chemical shifts are reported in parts per million (ppm) and are relative to $CDCl_3$ (7.26 ppm and 77.0 ppm), CD_3OD (3.31 ppm and 49.0 ppm), DMSO-d_6 (2.50 ppm and 39.5 ppm) or D_2O (4.80 ppm). The abbreviations used are as follows: s, singlet; brs, broad singlet; d, doublet; dd, double of doublets; dt, doublet of triplets; t, triplet; q, quartet; qui, quintet; m, multiplet; and brm, broad multiplet. Coupling constants (J) are reported in Hertz (Hz). Thin-layer chromatography (TLC) was performed on aluminium backed silica plates (silica gel 60 F254, Merck, Darmstadt, Germany). Spots were visualized by UV detector (l: 254 nm) and/or by staining and warming with phosphomolybdic acid (5% w/v solution in EtOH). When required, flash chromatographic purifications were performed using Biotage Isolera (Biotage AB, Uppsala, Sweden). Melting points were determined using a Buchi 535 electrothermal apparatus. Purity of target compounds was >95%. HPLC analyses were performed on a Shimadzu (Kyoto, Japan) LC-20A Prominence equipped with a CBM-20A communication bus module, two LC-20AD dual piston pumps, an SPD-M20A photodiode array detector, and a Rheodyne 7725i injector (Rheodyne Inc., Cotati, CA, USA) with a 20-μL stainless steel loop. A GraceSmart RP18 column (Grace, Sedriano, Italy, 250 × 4.6 mm i.d., 5 mm, 100 Å) was used as the analytical column. A Varian 385-LC evaporative light scattering detector (ELSD) (Agilent Technologies, Santa Clara, CA, USA) was utilized for the analyses. The analog-to-digital conversion of the output signal from the ELSD was allowed by a common interface device. The adopted ELSD conditions were: T_{vap} = 70 °C, T_{neb} = 50 °C, gas flow = 1.0 L min^{-1}, gain = 1. The HPLC analyses were performed at 1.0 mL min^{-1} eluent flow rate, after previous conditioning by passing through the column the selected mobile phase for at least 30 min at the same eluent velocity. Before use, all the mobile phases were always filtered through a 0.22 mm Millipore filter (Bedford, MA – USA) and then degassed with 20 min sonication. The column temperature was controlled through a heather/chiller thermostat (Grace 7956 R, Grace, Sedriano, Italy). All the analyses were performed at a 25 °C column temperature using analytical grade MeCN and ultrapure water (σ = 18.3 MΩ x cm) obtained through New Gradient. The following gradient was used: H_2O (NH_4HCO_2 40 mM, pH 2.5)/MeCN 60:40 (v/v), 6 min → H_2O (NH_4HCO_2 40 mM, pH 2.5)/MeCN 50:50 (v/v), ramp 1 min, then isocratic H_2O (NH_4HCO_2 40 mM, pH 2.5)/MeCN 50:50 (v/v), 26 min. Detector: ELSD (T_{vap} 70 °C, T_{neb} 50 °C, gas flow 1 L min^{-1}). High resolution mass spectrometry (HRMS) measurements were recorded on Agilent 6500 Q-TOF series instrument (Agilent technologies, USA). The MS system was set with an electrospray ionization source (ESI) in the negative mode with optimized parameters. MassHunter software version B.05.01 (Agilent Technology) was used to control the LC–MS/MS system, for data prediction, acquisition, analysis, and processing. Samples were dissolved in MeOH.

4.1.2. Synthesis

4.1.2.1. 24,24-Diphenyl 3α,7α-dihydroxy-6α-ethyl-5β-cholan-23-ene (4a). To a solution of compound **2** (10 g, 23.8 mmol) in MeOH (100 mL), p-TSA-H_2O (0.45 g, 0.24 mmol) was added, and the mixture was sonicated for 2 h. The mixture was then concentrated under reduced pressure, and the resulting residue was dissolved in CH_2Cl_2 (300 mL), washed with saturated aqueous $NaHCO_3$ solution (200 mL), H_2O (200 mL) and brine (200 mL). The organic phase was dried over anhydrous Na_2SO_4 and concentrated under reduced pressure. The crude thus obtained (quantitative recovery) was dissolved in dry THF (80 mL) and a 3 M solution of phenylmagnesium bromide in Et_2O (80 mL, 238 mmol) was added dropwise over 15 min. The resulting solution was refluxed overnight. The reaction was cooled to room temperature and 3 N aqueous HCl (200 mL) was slowly added. The mixture was extracted with CH_2Cl_2 and the combined organic layers were dried over anhydrous Na_2SO_4 and concentrated under reduced pressure to give a crude brown oil (20 g). The residue was dissolved in EtOH (50 mL) and treated with 3 N aqueous HCl (25 mL). After stirring at 50 °C for 4 h, the reaction mixture was concentrated in vacuo and diluted with H_2O (100 mL). The aqueous phase was extracted with CH_2Cl_2, and the combined organic layers were dried over anhydrous Na_2SO_4 and concentrated under reduced pressure. The crude was purified by flash chromatography (Eluent: $CHCl_3$/MeOH) to give the desired product 24,24-diphenyl 3α,7α-dihydroxy-6α-ethyl-5β-cholan-23-ene (**4a**) (10.3 g, 19.1 mmol, 80% yield) as a pale yellow oil. ^{1}H NMR ($CDCl_3$, 400 MHz): δ 0.67 (s, 3H, 18-CH_3), 0.89–0.93 (m, 6H, 19-CH_3 + 6-CH_2CH_3), 0.99 (d, J = 6.60 Hz, 3H, 21-CH_3), 2.23–2.29 (brm, 1H, 22-CH_2), 3.37–3.52 (m, 1H, 3β-CH), 3.70 (s, 1H, 7β-CH), 6.12 (t, J = 6.50 Hz, 1H, 23-CH), 7.16–7.45 (brm, 10H, 2 x C_6H_5). ^{13}C NMR ($CDCl_3$, 100.6 MHz): δ 11.6, 11.8, 19.1, 20.7, 22.2, 23.1, 23.7, 28.2, 30.6, 33.2, 34.0, 35.5 (x2), 36.0, 36.9, 39.5, 40.0, 41.2, 42.8, 45.2, 50.5, 50.8, 55.9, 70.9, 72.4, 77.2, 115.3, 120.5, 126.7 (x2), 127.1, 128.0, 128.8, 129.6, 130.0, 140.4, 142.2, 143.0.

4.1.2.2. 24,24-Diphenyl 3α-acetoxy-7α-hydroxy-6α-ethyl-5β-cholan-23-ene (4b). To a solution of compound **4a** (10.3 g, 19.1 mmol) in THF (100 mL), pyridine (2.5 mL, 30.5 mmol), DMAP (0.6 g, 4.8 mmol) and Ac_2O (2.2 mL, 22.9 mmol) were sequentially added and the resulting mixture was stirred at 25 °C for 8 h. The mixture was diluted with CH_2Cl_2 (200 mL), washed with 3 N aqueous HCl (200 mL), saturated aqueous $NaHCO_3$ solution (200 mL), H_2O (200 mL), brine (200 mL), dried over anhydrous Na_2SO_4 and concentrated under reduced pressure. The crude (white solid, nearly quantitative recovery) was used for the next step without further purification. ^{1}H NMR ($CDCl_3$, 400 MHz): δ 0.65 (s, 3H, 18-CH_3), 0.90 (t, J = 7.34 Hz, 3H, 6-CH_2CH_3), 0.95 (s, 3H, 19-CH_3), 0.97 (d, J = 6.56 Hz, 3H, 21-CH_3), 2.05 (s, 3H, 3-CO_2CH_3), 2.23–2.32 (brm, 1H, 22-CH_2), 3.69 (s, 1H, 7β-CH), 4.55–4.61 (m, 1H, 3β-CH), 6.11 (t, J = 6.28 Hz, 1H, 23-CH), 7.11–7.39 (brm, 10H, 2 x C_6H_5). ^{13}C NMR ($CDCl_3$, 100.6 MHz): δ 11.6, 11.7, 19.1, 20.7, 21.3, 21.5, 22.2, 23.1, 23.9, 26.8, 28.1, 29.0, 34.1, 35.2, 35.5, 36.0, 36.9, 38.9, 39.3, 41.0, 42.9, 44.9, 50.5, 55.9, 73.2, 74.6, 77.2, 121.5, 125.8, 126.7 (x2), 127.1, 128.0, 128.1, 128.9, 129.4, 130.0, 140.4, 142.2, 142.9, 170.4, 170.6.

4.1.2.3. Ozonolysis reaction under flow conditions. A solution of compound **4a** or **4b** (5 mmol) in CH_2Cl_2/MeOH (42 mL, 1:1, v/v) was pumped with a flow rate of 1 mL min^{-1} to be mixed with a stream of ozone (1 L min^{-1}) and flowed through a reactor coil (FEP, V = 50 mL, τ = 6 min) at 0 °C. The reactor output was purged with nitrogen and was poured into a round bottom flask containing a stirred methanolic solution of $NaBH_4$ (0.76 g, 20 mmol). The reaction mixture was then quenched with 3 N aqueous HCl (40 mL) and the phases were separated. The organic layer was washed with H_2O (40 mL), brine (40 mL), dried over Na_2SO_4 and concentrated under vacuum. The crude **6a** was crystallized from *tert*-butyl methyl ether while **6b** was purified by flash

automated chromatography (Eluent: petroleum ether/EtOAc). **6a:** White solid (m.p.: 153–154 °C). Isolated yield: 90% (1.76 g, 4.52 mmol). ^{1}H NMR ($CDCl_3$, 400 MHz): δ 0.66 (s, 3H, 18-CH_3), 0.87–0.92 (m, 6H, 6-CH_2CH_3 + 19-CH_3), 0.92–0.96 (m, 3H, 21-CH_3), 3.36–3.47 (m, 1H, 3β-CH), 3.61–3.68 (m, 1H, 7β-CH), 3.70 (m, 2H, 23-CH_2OH). ^{13}C NMR (CD_3OD, 100.6 MHz): δ 12.9, 13.1, 20.2, 22.8, 24.4, 24.6, 25.4, 30.3, 32.1, 35.0, 35.3, 35.4, 37.5, 37.6, 40.7, 41.9, 42.4, 44.0, 44.6, 47.8, 52.5, 58.8, 61.7, 72.0, 74.0. **6b:** White solid. Isolated yield: 88% (1.90 g, 4.41 mmol). ^{1}H NMR ($CDCl_3$, 400 MHz): δ 0.66 (s, 3H, 18-CH_3), 0.86–0.92 (m, 6H, 6-CH_2CH_3 + 19-CH_3), 0.95 (d, 3H, J = 6.50 Hz, 21-CH_3), 1.95 (s, 3H, CH_3CO), 3.59–3.63 (m, 1H, 7β-CH), 3.66–3.72 (m, 2H, 23-CH_2OH), 4.42–4.55 (m, 1H, 3β-CH). ^{13}C NMR ($CDCl_3$, 100.6 MHz): δ 11.8, 11.9, 19.0, 20.9, 21.7, 22.3, 23.2, 23.9, 26.8, 28.5, 29.8, 33.0, 33.3, 35.3, 35.73, 39.1, 39.7, 40.1, 41.3, 42.3, 45.2, 50.7, 56.5, 61.0, 70.9, 74.8, 170.9.

4.1.2.4. 3α,7α-dihydroxy-6α-ethyl-24-nor-5β-cholan-23-sulfate sodium salt (INT-767, 1). Compound **6b** (5 g, 11.4 mmol) was dissolved in dry pyridine (150 mL) and treated with pyridine sulfur trioxide complex (pyr·SO_3) (2.4 g, 14.8 mmol) at 25 °C for 16 h. The crude was evaporated under vacuo and the residue thus obtained was dissolved in NaOH/MeOH (10% w/v, 150 mL) and heated at reflux for 28 h. The crude was concentrated under reduced pressure and purified by automated flash chromatography (RP-18; Eluent: H_2O/MeCN) to give **1** (4.40 g, 8.90 mmol, 78% yield) as white solid (m.p.: 206–207 °C). ^{1}H NMR (CD_3OD, 400 MHz): δ 0.71 (s, 3H, 18-CH_3), 0.89–0.92 (m, 6H, 19-CH_3 + 6-CH_2CH_3), 1.00 (d, J = 6.38 Hz, 3H, 21-CH_3), 2.00–2.03 (m, 2H, 22-CH_2), 3.31–3.35 (m, 1H, 3β-CH), 3.66 (s, 1H, 7β-CH), 4.01–4.07 (brm, 2H, 23-CH_2). ^{13}C NMR (CD_3OD, 100.6 MHz): δ 10.6, 10.7, 17.7, 20.5, 22.1, 22.3, 23.1, 27.9, 29.8, 32.8, 33.0, 33.1, 35.1, 35.2, 35.4, 39.6, 40.1, 41.7, 42.4, 45.6, 50.2, 56.4, 65.7 (3-CH), 69.7 (23-CH_2), 71.8 (7-CH). HPLC-ELSD purity: >95% (r.t.: 12.58 min). HRMS *m/z* [M − H]$^-$ calcd for $C_{25}H_{44}O_6S$: 471.27856; found: 471.27912; Δppm = +1.19.

4.1.2.5. INT-767 3β-D-glucuronide methyl ester-triacetate (11). To suspension of INT-767 (**1**) (750 mg, 1.5 mmol) in anhydrous toluene (75 mL) molecular sieves (0.75 g, 4 Å, 325 mesh), methyl 2,3,4-tri-O-acetyl-α-D-glucopyranosyluronate bromide (**10**) (1.8 g, 4.6 mmol) and Fetizon's reagent (16.84 g, loading 0.9 mmol Ag_2CO_3 g^{-1}, 10 eq.) were added and the resulting suspension was stirred at 25 °C under argon atmosphere and in the dark for 40 h [43]. The suspension was filtered over Celite and the filtrate was concentrated under reduced pressure. The crude was purified by automated flash chromatography on silica (Eluent: CH_2Cl_2/MeOH from 100:0 to 85:15, v/v) affording the desired INT-767 3β-D-glucuronide methyl ester-triacetate (**11**) (935 mg, 1.18 mmol, 78% yield) as white solid. ^{1}H NMR ($CDCl_3$, 400 MHz) δ: 0.65 (s, 3H, 18-CH_3), 0.86–0.90 (m, 6H, 19-CH_3 + 6-CH_2CH_3), 0.96 (d, J = 6.50 Hz, 3H, 21-CH_3), 2.01–2.05 (m, 9H, 3 x $OCOCH_3$), 3.42–3.48 (m, 1H, 3-CH), 3.67 (brs, 1H, 7-CH), 3.75 (s, 3H,CO_2CH_3), 4.03 (d, 1H, J = 9.20 Hz, 5′-CH), 4.02–4.20 (m, 2H, 23-CH_2), 4.67 (d, J = 7.62 Hz, 1H, 1′-CH), 4.92–4.96 (m, 1H, 2′-CH), 5.19–5.27 (m, 2H, 3′-CH + 4′-CH).

4.1.2.6. INT-767 3β-D-glucuronide disodium salt (7). To a solution of compound **11** (0.93 g, 1.2 mmol) in MeOH (17 mL), Na_2CO_3•$10H_2O$ (6.75 g, 23.6 mmol) was added and the resulting suspension was stirred at 25 °C for 72 h. The solvent was removed under reduced pressure and the crude was purified by RP-18 automated flash chromatography (Eluent: H_2O/MeOH) affording **7** (076 mg, 1.1 mmol, 92% yield) as white solid (m.p.: >220 °C, dec). ^{1}H NMR (DMSO-d_6, 400 MHz) δ: 0.61 (s, 3H, 18-CH_3), 0.81–0.84 (m, 6H, 19-CH_3 + 6-CH_2CH_3), 0.88 (d, J = 6.50 Hz, 3H, 21-CH_3), 3.00–3.15 (m, 3H, 2′-CH + 3′-CH + 4′-CH), 3.35–3.45 (m, 1H, 3-CH), 3.51 (brs, 1H, 7-CH), 3.61–3.75 (m, 2H, 23-CH_2), 4.02–4.08 (m, 1H, 5′-CH), 4.17 (d, J = 7.16 Hz, 1H, 1′-CH). ^{13}C NMR (DMSO-d_6, 100.6 MHz) δ: 12.1, 12.2, 18.9, 20.8, 22.5, 23.4, 23.5, 26.2, 28.3, 31.1, 31.3, 32.9, 35.4, 35.6, 35.8, 40.3, 40.5, 41.7, 42.5, 45.9, 50.5, 56.4, 63.8 (23-CH_2), 68.6 (3′-CH), 72.6 (5′-CH), 73.8 (7-CH), 74.0 (3-CH), 76.4 (4′-CH), 77.1 (2′-CH), 99.6 (6′-CH), 173.5 (CO_2Na). HRMS *m/z* [M − H]$^-$ calcd for $C_{31}H_{52}O_{12}S$: 648.3179; found: 648.4258.

4.1.2.7. 3α-hydroxy-7α-acetoxy-6α-ethyl-24-nor-5β-cholan-23-sulfate (12). To a suspension of INT-767 (**1**) (5 g, 10.11 mmol) in CH_2Cl_2 (180 mL) were added Ac_2O (9.55 mL, 101.1 mmol) and $Bi(OTf)_3$ (0.33 g, 0.51 mmol) and the resulting suspension was stirred at 25 °C for 3 h. A saturated aqueous $NaHCO_3$ solution (50 mL) was added dropwise and the phases were separated. The aqueous phase was extracted with CH_2Cl_2, and the combined organic extracts were washed with H_2O (40 mL), brine (40 mL), dried over Na_2SO_4 and concentrated under vacuum. The crude mixture (nearly quantitative recovery) was dissolved in MeOH and treated with NaOH (1.2 g, 30 mmol). The resulting mixture was stirred at 25 °C for 1 h. The solvent was evaporated under reduced pressure and the crude was purified by RP-18 automated flash chromatography (Eluent: H_2O/MeOH) affording the desired 3α-hydroxy-7α-acetoxy-6α-ethyl-24-*nor*-5β-cholan-23-sulfate (**12**) (4.56 g, 8.5 mmol, 85% yield from **1**) as white solid. ^{1}H NMR (CD_3OD, 400 MHz) δ: 0.70 (s, 3H, 18-CH_3), 0.90–0.99 (m, 9H, 19-CH_3 + 21-CH_3 + 6-CH_2CH_3), 2.06 (s, 3H, $OCOCH_3$), 3.33–3.39 (m, 1H, 3-CH), 3.95–4.05 (m, 2H, 23-CH_2), 5.09 (brs, 1H, 7-CH). ^{13}C NMR (CD_3OD, 100.6 MHz) δ: 10.6, 10.7, 17.7, 19.7, 20.4, 22.1, 22.2, 23.5, 27.7, 29.8, 32.4, 32.7, 34.1, 35.1 (x3), 38.8, 39.3, 41.0, 42.64, 45.1, 50.5, 56.0, 65.6, 71.2, 73.4, 171.1.

4.1.2.8. 3α-oxo-7α-hydroxy-6α-ethyl-24-nor-5β-cholan-23-sulfate sodium salt (9). To a suspension of compound **12** (1.5 g, 2.8 mmol) in anhydrous CH_2Cl_2 (90 mL), Dess-Martin periodinane (3.5 g, 8.4 mmol) was added at 25 °C under argon atmosphere. The resulting suspension was stirred at 25 °C for 18 h. The reaction was quenched by adding 5% (wt) aqueous solution of $Na_2S_2O_3$ (200 mL) and extracted with CH_2Cl_2. The combined organic extracts were dried over anhydrous Na_2SO_4 and concentrated under reduced pressure. The crude was dissolved in MeOH (5 mL), 20% (wt) aqueous solution of NaOH (5 mL) was added and the mixture was refluxed for 48 h. The solvent was removed under vacuo and the crude mixture was purified by RP-18 automated flash chromatography (Eluent: H_2O/MeOH) affording the desired 3α-oxo-7α-hydroxy-6α-ethyl-24-*nor*-5β-cholan-23-sulfate sodium salt (**9**) (1.05 g, 2.1 mmol, 48% yield) as white solid (m.p.: 180–182 °C). ^{1}H NMR (CD_3OD, 400 MHz) δ: 0.75 (s, 3H, 18-CH_3), 0.92 (t, J = 7.32 Hz, 3H, 6-CH_2CH_3), 1.01–1.03 (m, 6H, 21-CH_3 + 19-CH_3), 2.49 (m, 1H, 4α-CH), 3.23 (m, 1H, 4β-CH), 3.73 (s, 1H, 7-CH), 4.06 (m, 2H, 23-CH_2). ^{13}C NMR (CD_3OD, 100.6 MHz) δ: 11.7, 12.1, 19, 22.1, 22.5, 23.1, 24.3, 29.2, 34.1, 34.7, 36.4, 36.7, 37.5, 38.0, 40.8, 41.3, 41.4, 42.9, 43.7, 51.4, 57.6, 67.0 (23-CH_2), 70.8 (7-CH), 216.7 (3-C═O). HRMS *m/z* [M − H]$^-$ calcd for $C_{25}H_{42}O_6S$: 470.2702; found: 470.3598.

4.1.2.9. 7α-hydroxy-6α-ethyl-24-nor-5β-cholan-3α,23-disulfate sodium salt (8). To a solution of INT-767 (**1**) (1.5 g, 3.0 mmol) in dry pyridine (23 mL), pyridine sulfur trioxide complex (pyr·SO_3) (1.4 g, 9 mmol) was added at room temperature and the resulting mixture was stirred for 48 h. The crude was evaporated under vacuo and the residue thus obtained was dissolved in NaOH/MeOH (10% w/v, 150 mL) and refluxed for 36 h. The crude was concentrated under reduced pressure and purified by automated flash chromatography (RP-18; Eluent: H_2O/MeCN) to give the desired 7α-hydroxy-6α-ethyl-24-*nor*-5β-cholan-3α,23-disulfate sodium salt (**8**) (1.1 g, 1.8 mmol, 61%) as white solid (m.p.: 210–212 °C, dec.). ^{1}H NMR (D_2O, 400 MHz) δ: 0.58 (s, 3H, 18-CH_3), 0.78–0.82 (m, 6H, 19-CH_3 + 6-CH_2CH_3), 0.90 (d, J = 5.13 Hz, 3H, 21-CH_3), 3.63 (brs, 1H, 7-CH), 3.94–4.05 (m, 3H, 3-CH + 23-CH_2). ^{13}C NMR (D_2O, 100.6 MHz) δ: 12.5 (x 2), 13.0, 19.7, 22.1, 23.1, 24.3, 24.7, 28.6, 29.3, 31.5, 34.3, 34.5, 35.9, 36.4, 40.5, 41.1, 42.7, 43.7, 46.1, 51.4, 56.5, 68.9 (23-CH), 71.9 (7-CH), 82.9 (3-CH). HRMS *m/z* [M − H]$^-$ calcd for $C_{25}H_{44}O_9S_2$: 552.2427; found: 552.3482.

4.2. Biology

Activation of the FXR receptor was determined using a recruitment coactivator assay, namely, AlphaScreen technology. Briefly, assays were conducted in white, low volume, 384-well ProxyPlate using a final volume of 10 μL containing 10 nM glutathione transferase-tagged hFXR-LBD protein and 30 nM biotinylated Src-1 peptide. The stimulation was carried out with different bile acid derivatives concentrations for 30 min at 25 °C. Luminescence was read in an EnVision 2103 microplate analyzer (PerkinElmer, USA) after incubation with the detection mix (acceptor and donor beads) for 4 h at 25 °C in the dark. Dose-response curves were conducted in triplicate. TGR5 activation was evaluated by measuring the level of intracellular cAMP using a HTR-FRET assay (Lance kit - PerkinElmer) according to the manufacturer's protocol. NCI–H716 cells were cultured on 96-well plates coated with Matrigel 0.75 mg/mL; BD Biosciences) in DMEM supplemented with 10% FCS, 100 units/ml penicillin, and 100 μg/mL streptomycin sulfate, after 24 h, the cells were stimulated with dose response of compounds for 1 h at 37 °C in OptiMEM containing 1 mM of 3-isobutyl-1-methylxanthine. The plate was read in EnVision microplate analyzer (PerkinElmer Life and Analytical Sciences).

4.3. Molecular docking

The crystallographic structure of FXR with PDB code 1OSV was selected as template of the ligand binding domain (LBD) of the receptor for docking studies of the compounds [44]. In addition, the cryo-electron microscopy (EM) structure of TGR5 (PDB code 7CFN) [48] was selected for docking studies of the compounds into the G-protein coupled receptor of bile acids. These structures were retrieved from the Research Collaboratory for Structural Bioinformatics (RCSB, http://www.rcsb.org/; access date April 2022) and processed employing the Protein Preparation Wizard (PPW) tool, as implemented in Maestro (Schrödinger Release 2021-3: Maestro v12.9, Schrödinger, LLC, New York, NY, 2021) [54]. Specifically, missing residues were inserted with Prime (Schrödinger Release 2021-3: Prime, Schrödinger, LLC, New York, NY, 2021) and hydrogen atoms were added sampling water orientation and optimizing the hydrogen bond network with PROPKA [55,56] Internal geometries of protein atoms and bonds were then optimized restraining the atomic coordinate of heavy atoms with a with a Root Mean Square Distance (RMSD) convergence criterion of 0.3 Å. Compounds were designed with Maestro and their geometry was optimized using LigPrep (Schrödinger Release 2021-3: LigPrep, Schrödinger, LLC, New York, NY, 2021). In particular, compounds were considered in their ionization state at the target pH of 7 ± 2. All geometry refinements of protein and compound structures were carried out using the OPLS4 force field with a convergence criterion of energy minimization gradient set to 0.05 kJ/Å-mol [57]. Docking studies were performed using Glide (Schrödinger Release 2021-3: Glide v12.9, Schrödinger, LLC, New York, NY, 2021 Glide v12.9, Schrödinger, LLC, New York, NY, USA) [58,59], with the standard precision (SP) scoring function and setting twice the enhanced sampling functionality for a thorough conformational sampling of the compounds. The grid box was defined considering the binding poses of the co-crystallized ligands in chain A and chain B of 1OSV (chain A grid center: 11.688, 37.427, 16.762; chain B grid center: 15.080, 18.048, 57.906), as well as 7CFN (grid center: −9.283 27.736 13.600). In this latter case, only the main binding pose of INT-777 was considered which is located in the middle of the seven helical bundle of 7CFN. The inner and outer boxes of each grid were sized 10 × 10 × 10 Å and 30 × 30 × 30 Å, respectively. At most 5 output docking poses for each ligand were saved from docking calculations and ranked according to three different estimations of the ligand binding free energy: SP Gscore, Emodel score for pose selection, and the molecular mechanics-generalized Born surface area (MMGBSA) score which was calculated using Prime (Schrödinger Release 2021-3: Prime v12.9, Schrödinger, LLC, New York, NY, 2021). In particular, the calculation of ligand binding free energies with MMGBSA was carried out using the OPLS4 force field and a Variable-dielectric generalized Born (VSGB) solvation water model. SiteMap (Schrödinger Release 2021-3: SiteMap v12.9, Schrödinger, LLC, New York, NY, 2021) was used to calculate binding site properties and generate solvent accessible surfaces representing the interaction property complementarity with the ligands [58,59].

Author contributions

The manuscript was written through contributions of all authors. All authors have given approval to the final version of the manuscript.

Declaration of competing interest

The authors declare the following financial interests/personal relationships which may be considered as potential competing interests: Antimo Gioiello reports financial support was provided by Intercept Pharmaceuticals Inc. Antimo Gioiello and Roberto Pellicciari has patent issued to Intercept Pharmaceuticals.

Data availability

Data will be made available on request.

Acknowledgment

We gratefully acknowledge financial support by TES Pharma (Perugia, Italy) and Intercept Pharmaceuticals (New York, USA).

Appendix A. Supplementary data

Supplementary data to this article can be found online at https://doi.org/10.1016/j.ejmech.2022.114652.

Abbreviations

CDCA	chenodeoxycholic acid
DCC	N,N′-dicyclohexylcarbodiimide
EM	electron microscopy
FXR	farnesoid X receptor
3α-HSD	3α-hydroxysteroid dehydrogenase
HTR-FRET	homogeneous time-resolved fluorescence resonance energy transfer
LBD	ligand binding domain
LCA	lithocholic acid
MMGBSA	molecular mechanics-generalized Born surface area
NAFLD	non alcoholic fatty liver disease
NASH	non alcoholic steato hepatitis
OCA	obeticholic acid
P	pocket
PBC	primary biliary cirrhosis
PD	pharmacodynamics
PK	pharmacokinetics
PPW	protein preparation wizard
TGR5	Takeda-G-protein-receptor-5

References

[1] G. Rizzo, D. Passeri, F. De Franco, G. Ciaccioli, L. Donadio, G. Rizzo, S. Orlandi, B. Sadeghpour, X.X. Wang, T. Jiang, M. Levi, M. Pruzanski, L. Adorini, Functional characterization of the semisynthetic bile acid derivative INT-767, a dual farnesoid X receptor and TGR5 agonist, Mol. Pharmacol. 78 (2010) 617–630.

[2] R. Pellicciari, A. Gioiello, The discovery of bbeticholic Acid (Ocaliva™): first-in-class FXR agonist, in: J. Fischer, C. Klein, W.E. Childers (Eds.), Successful Drug Discovery, Wiley-VCH Verlag GmbH & Co. KGaA, 2018, pp. 197–244.

[3] C. Thomas, A. Gioiello, L. Noriega, A. Strehle, J. Oury, G. Rizzo, A. Macchiarulo, H. Yamamoto, C. Mataki, M. Pruzanski, R. Pellicciari, J. Auwerx, K. Schoonjans,

TGR5-mediated bile acid sensing controls glucose homeostasis, Cell Metabol. 10 (2009) 167–177.
[4] T.W.H. Pols, M. Nomura, T. Harach, G. Lo Sasso, M.H. Oosterveer, C. Thomas, G. Rizzo, A. Gioiello, L. Adorini, R. Pellicciari, J. Auwerx, K. Schoonjans, TGR5 activation inhibits atherosclerosis by reducing macrophage inflammation and lipid loading, Cell Metabol. 14 (2011) 747–757.
[5] A. Perino, L.A. Velázquez-Villegas, N. Bresciani, Y. Sun, Q. Huang, V.S. Fénelon, A. Castellanos-Jankiewicz, P. Zizzari, G. Bruschetta, S. Jin, A. Baleisyte, A. Gioiello, R. Pellicciari, J. Ivanisevic, B.L. Schneider, S. Diano, D. Cota, K. Schoonjans, Central anorexigenic actions of bile acids are mediated by TGR5, Nat. Metab. 3 (2021) 595–603.
[6] A. Roda, R. Pellicciari, A. Gioiello, F. Neri, C. Camborata, D. Passeri, F. De Franco, S. Spinozzi, C. Colliva, L. Adorini, M. Montagnani, R. Aldini, Semisynthetic bile acid FXR and TGR5 agonist: physicochemical properties, pharmacokinetics, and metabolism in the rat, J. Pharmacol. Exp. Therapeut. 350 (2014) 56–68.
[7] J.D. Roth, M. Feigh, S.S. Veidal, L.K.D. Fensholdt, K.T. Rigbolt, H.H. Hansen, L. C. Chen, M. Petitjean, W. Friley, N. Vrang, J. Jelsing, M. Young, INT-767 improves histopathological features in a diet-induced ob/ob mouse model of biopsy-confirmed non-alcoholic steatohepatitis, World J. Gastroenterol. 24 (2018) 195–210.
[8] R.H. McMahan, X.X. Wang, L.L. Cheng, T. Krisko, M. Smith, K. El Kasmi, M. Pruzanski, L. Aldorini, L. Golden-Mason, M. Levi, H.R. Rosen, Bile acid receptor activation modulates hepatic monocyte activity and improves nonalcoholic fatty liver disease, J. Biol. Chem. 17 (2013) 11761–11770.
[9] X. Wang, L. Qiu, S. Hazra, Q. Li, L. Adorini, M. Pruzanski, M.B. Grant, M. Levi, Dual Activation of FXR and TGR5 Protects from Diabetic Nephropathy and Retinopathy in Mouse Model of Type 1 Diabetes, American Diabetes Association (ADA) 73rd Scientific Sessions, Chicago, Illinois, 2013. June 21-25.
[10] A. Baghdasaryan, T. Claudel, J. Gumhold, D. Silbert, L. Adorini, A. Roda, S. Vecchiotti, F.J. Gonzalez, K. Schoonjans, M. Strazzabosco, P. Fickert, M. Trauner, Dual farnesoid X receptor/TGR5 agonist INT-767 reduces liver injury in the Mdr2-/- (Abcb4-/-) mouse cholangiopathy model by promoting biliary HCO_3 output, Hepatology 54 (2011) 1303–1312.
[11] E. Canovai, R. Farré, A. Accarie, G. De Hertogh, T. Vanuytsel, J. Pirenne, L. J. Ceulemans, INT 767 – a novel dual farnesoid-x-receptor (FXR) and Takeda G-protein receptor (TGR5) agonist attenuates intestinal ischemia reperfusion injury, Transplantation 104 (2020) S167–S168.
[12] P. Comeglio, I. Cellai, T. Mello, S. Filippi, E. Maneschi, F. Corcetto, C. Corno, E. Sarchielli, A. Morelli, E. Rapizzi, D. Bani, D. Guasti, G.B. Vannelli, A. Galli, L. Adorini, M. Maggi, L. Vignozzi, INT-767 prevents NASH and promotes visceral fat brown adipogenesis and mitochondrial function, J. Endocrinol. 238 (2018) 107–127.
[13] Y.-B. Hu, X.-Y. Liu, W. Zhan, Farnesoid X receptor agonist INT-767 attenuates liver steatosis and inflammation in rat model of nonalcoholic steatohepatitis, Drug Des. Dev. Ther. 12 (2018) 2213–2221.
[14] S. Miyazaki-Anzai, M. Masuda, M. Levi, A.L. Keenan, M. Miyazaki, Dual activation of the bile acid nuclear receptor FXR and G-protein-coupled receptor TGR5 protects mice against atherosclerosis, PLoS One 9 (2014), e108270.
[15] C. D'Amore, F.S. Di Leva, V. Sepe, B. Renga, C. Del Gaudio, M.V. D'Auria, A. Zampella, S. Fiorucci, V. Limongelli, Design, synthesis, and biological evaluation of potent dual agonist of nuclear and membrane bile acid receptors, J. Med. Chem. 57 (2014) 937–954.
[16] A. Radomińska-Pyrek, T. Huynh, R. Lester, J. St Pyrek, Preparation and Characterization of 3-monohydroxylated bile acids of different side chain length and configuration at C-3. Novel approach to the synthesis of 24-norlithocholic acid, J. Lip. Res. 27 (1986) 102–113.
[17] A.K. Batta, S.C. Datta, G.S. Tint, D.S. Alberts, D.L. Earnest, G. Salen, A convenient synthesis of dinorbile acids: oxidative hydrolysis of norbile acid nitriles, Steroids 64 (1999) 780–784.
[18] G.L. Carlson, D.T.E. Belobaba, A.F. Hofmann, Y. Wedmid, 24-nor-5β-chol-22-enes derived from the major bile acids by oxidative decarboxylation, Steroids 30 (1977) 787–793.
[19] W.M. Hoehn, H.L. Mason, The degradation of desoxycholic acid to etio-desoxycholic acid through etio-desoxycholyl methyl ketone, J. Am. Chem. Soc. 60 (1938) 1493–1497.
[20] Department of Health - the State of New Jersey, 2005, 12 May 2022, https://nj.gov/health/eoh/rtkweb/documents/fs/0437.pdf.
[21] S.G. Van Ornum, R.M. Champeau, R. Pariza, Ozonolysis applications in drug synthesis, Chem. Rev. 106 (2006) 2990–3001.
[22] D. Dallinger, B. Gutmann, C.O. Kappe, The concept of chemical generators: on-site on-demand production of hazardous reagents in continuous flow, Acc. Chem. Res. 53 (2020) 1330–1341.
[23] H. Ishitani, Y. Saito, B. Laroche, X. Rao, S. Kobayashi, Recent perspectives in catalysis under continuous flow, in: V.L. Santiago, E. Garcia-Verdugo (Eds.), Flow Chemistry: Integrated Approaches for Practical Applications, RSC, 2019, pp. 1–49.
[24] R. Ricciardi, J. Huskens, W. Verboom, Nanocatalysis in flow, ChemSusChem 8 (2015) 2586–2605.
[25] M.D. Roydhouse, A. Ghaini, A. Constantinou, A. Cantu-Perez, W.B. Motherwell, A. Gavriilidis, Ozonolysis in flow using capillary reactors, Org. Process Res. Dev. 15 (2011) 989–996.
[26] M.O. Kitching, O.E. Dixon, M. Baumann, I.R. Baxendale, Flow synthesis and bio-pharmacological studies of a P2X7 antagonist that shows analgesic activity, Eur. J. Org Chem. 44 (2017) 6540–6553.
[27] C. Battilocchio, L. Guetzoyan, C. Cervetto, L.D.C. Mannelli, D. Frattaroli, I. R. Baxendale, G. Maura, L. Sautebin, M. Biava, C. Ghelardini, M. Marcoli, S.V. Ley, A.C.S. Med, Chem. Lett. 4 (2013) 704–709.
[28] A. Gioiello, A. Piccinno, A.M. Lozza, B. Cerra, The medicinal chemistry in the era of machines and automation: recent advances in continuous flow technology, J. Med. Chem. 63 (2020) 6624–6647.
[29] B. Gutmann, D. Cantillo, C.O. Kappe, Continuous-flow technology - a tool for the safe manufacturing of active pharmaceutical ingredients, Angew. Chem. Int. Ed. 54 (2015) 6688–6728.
[30] M. Baumann, I.R. Baxendale, The synthesis of active pharmaceutical ingredients (APIs) using continuous flow chemistry, Beilstein J. Org. Chem. 11 (2015) 1194–1219.
[31] C.J. Mallia, I.R. Baxendale, The use of gases in flow synthesis, Org, Process Res. Dev. 20 (2016) 327–360.
[32] R.A. Al-Horani, U.R. Desai, Chemical sulfation of small molecules – advances and challenges, Tetrahedron 66 (2010) 2907–2918.
[33] L.S. Simpson, T.S. Widlanski, A comprehensive approach to the synthesis of sulfate esters, J. Am. Chem. Soc. 128 (2006) 1605–1610.
[34] E.E. Gilbert, Sulfonation and Related Reactions, Interscience, New York, 1966, pp. 1–30.
[35] Z. Zhang, W. Tang, Drug metabolism in drug discovery and development, Acta Pharm. Sin. B 8 (2018) 721–732.
[36] A.F. Hofmann, L.R. Hagey, Bile acids: chemistry, pathochemistry, biology, pathobiology, and therapeutics, Cell. Mol. Life Sci. 65 (2008) 2461–2483.
[37] J.L.Y. Chiang, Bile acid metabolism and signaling, Compr. Physiol. 3 (2013) 1191–1212.
[38] J.L.Y. Chiang, J.M. Ferrell, Bile acid metabolism in liver pathobiology, Gene Expr. 18 (2018) 71–87.
[39] M. Perreault, A. Białek, J. Trottier, M. Verreault, P. Caron, P. Milkiewicz, O. Barbier, Role of glucuronidation for hepatic detoxification and urinary elimination of toxic bile acids during biliary obstruction, PLoS One 8 (2013), e80994.
[40] T.M. Penning, Y. Jin, S. Steckelbroeck, T. Lanišnik Rižner, M. Lewis, Structure–function of human 3α-hydroxysteroid dehydrogenases: genes and proteins, Mol. Cell. Endocrinol. 215 (2004) 63–72.
[41] H. Eyssen, J. Van Eldere, G. Parmentier, S. Huijghebaert, J. Mertens, Influence of microbial bile salt desulfatation upon the fecal excretion of bile salt in gnotobiotics rats, J. Steroid Biochem. 22 (1985) 547–554.
[42] Y. Alnouti, Bile acid sulfation: a pathway of bile acid elimination and detoxification, Toxicol. Sci. 108 (2009) 225–246.
[43] S. Mostarda, F. Filipponi, R. Sardella, F. Venturoni, B. Natalini, R. Pellicciari, A. Gioiello, Glucuronidation of bile acids under flow conditions: design of experiments and Koenigs-Knorr reaction optimization, Org. Biomol. Chem. 12 (2014) 9592–9600.
[44] L.Z. Mi, S. Devarakonda, J.M. Harp, Q. Han, R. Pellicciari, T.M. Willson, S. Khorasanizadeh, F. Rastinejad, Structural basis for bile acid binding and activation of the nuclear receptor FXR, Mol. Cell. 11 (2003) 1093–1100.
[45] A. Macchiarulo, R. Nuti, G. Eren, R. Pellicciari, Charting the chemical space of target sites: insights into the binding modes of amine and amidine groups, J. Chem. Inf. Model. 49 (2009) 900–912.
[46] R. Pellicciari, G. Costantino, E. Camaioni, B.M. Sadeghpour, A. Entrena, T. M. Willson, S. Fiorucci, C. Clerici, A. Gioiello, Bile acid derivatives as ligands of the farnesoid X receptor. Synthesis, evaluation, and structure-activity relationship of a series of body and side chain modified analogues of chenodeoxycholic acid, J. Med. Chem. 47 (2004) 4559–4569.
[47] A. Macchiarulo, R. Pellicciari, Exploring the other side of biologically relevant chemical space: insights into carboxylic, sulfonic and phosphonic acid bioisosteric relationships, J. Mol. Graph. Model. 26 (2007) 728–739.
[48] F. Yang, C. Mao, L. Guo, J. Lin, Q. Ming, P. Xiao, X. Wu, Q. Shen, S. Guo, D.-D. Shen, R. Lu, L. Zhang, S. Huang, Y. Ping, C. Zhang, C. Ma, K. Zhang, X. Liang, Y. Shen, F. Nan, F. Yi, V.C. Luca, J. Zhou, C. Jiang, J.-P. Sun, X. Xie, X. Yu, Y. Zhang, Structural basis of GPBAR activation and bile acid recognition, Nature 587 (2020) 499–504.
[49] A. Macchiarulo, A. Gioiello, C. Thomas, T.W. Pols, R. Nuti, C. Ferrari, N. Giacchè, F. De Franco, M. Pruzanski, J. Auwerx, K. Schoonjans, R. Pellicciari, Probing the binding site of bile acids in TGR5, ACS Med. Chem. Lett. 4 (2013) 1158–1162.
[50] C.G.W. Gertzen, L. Spomer, S.H.J. Smits, D. Häussinger, V. Keitel, H. Gohlke, Mutational mapping of the transmembrane binding site of the G-protein coupled receptor TGR5 and binding mode prediction of TGR5 agonists, Eur. J. Med. Chem. 104 (2015) 57–72.
[51] A. Macchiarulo, A. Gioiello, C. Thomas, A. Massarotti, R. Nuti, E. Rosatelli, P. Sabbatini, K. Schoonjans, J. Auwerx, R. Pellicciari, Molecular field analysis and 3D-quantitative structure-activity relationship study (MFA 3D-QSAR) unveil novel features of bile acid recognition at TGR5, J. Chem. Inf. Model. 48 (2008) 1792–1801.
[52] R. Pellicciari, A. Gioiello, P. Sabbatini, F. Venturoni, R. Nuti, C. Colliva, G. Rizzo, L. Adorini, M. Pruzanski, A. Roda, A. Macchiarulo, Avicholic acid: a lead compound from birds on the route to potent TGR5 modulators, ACS Med. Chem. Lett. 3 (2012) 273–277.
[53] The Synthesis Was Scaled up to 30 G in Our Laboratory. The Route Was Then Adopted for the Kg-Scale Preparation Needed for Phase I Clinical Studies.
[54] H.M. Berman, J. Westbrook, Z. Feng, G. Gilliland, T.N. Bhat, H. Weissig, I. N. Shindyalov, P.E. Bourne, The protein data bank, Nucleic Acids Res. 28 (2000) 235–242.
[55] M.P. Jacobson, D.L. Pincus, C.S. Rapp, T.J.F. Day, B. Honig, D.E. Shaw, R. A. Friesner, A hierarchical approach to all-atom protein loop prediction, Proteins: Struct., Funct., Bioinf. 55 (2004) 351–367.

[56] M.P. Jacobson, R.A. Friesner, Z. Xiang, B. Honig, On the role of crystal packing forces in determining protein sidechain conformations, J. Mol. Biol. 320 (2002) 597–608.
[57] C. Lu, C. Wu, D. Ghoreishi, W. Chen, L. Wang, W. Damm, G. A. Ross, M. K. Dahlgren, E. Russell, C. D. Von Bargen, R. Abel, R. A. Friesner, E. D. Harder, OPLS4: improving force field accuracy on challenging regimes of chemical space, J. Chem. Theor. Comput. 17 (2021), 4291-4300.
[58] R.A. Friesner, J.L. Banks, R.B. Murphy, T.A. Halgren, J.J. Klicic, D.T. Mainz, M. P. Repasky, E.H. Knoll, M. Shelley, J.K. Perry, D.E. Shaw, P. Francis, P.S. Shenkin, Glide: a new approach for rapid, accurate docking and scoring. 1. Method and assessment of docking accuracy, J. Med. Chem. 47 (2004) 1739–1749.
[59] T.A. Halgren, R.B. Murphy, R.A. Friesner, H.S. Beard, L.L. Frye, W.T. Pollard, J. L. Banks, Glide: a new approach for rapid, accurate docking and scoring. 2. Enrichment factors in database screening, J. Med. Chem. 47 (2004) 1750–1759.